

RESEARCH ARTICLE

WILEY

River network travel time is correlated with dissolved organic matter composition in rivers of the contiguous United States

Jacob D. Hosen^{1,2,3}  | George H. Allen⁴  | Giuseppe Amatuli¹  |
 Sara Breitmeyer^{5,6}  | Matthew J. Cohen²  | Byron C. Crump⁷  | YueHan Lu⁸  |
 Jérôme P. Payet⁷  | Brett A. Poulin⁵  | Aron Stubbins⁹  |
 Byungman Yoon^{1,9}  | Peter A. Raymond¹ 

¹School of The Environment, Yale University, New Haven, Connecticut

²School of Forest Resources & Conservation, University of Florida, Gainesville, Florida

³Department of Forestry & Natural Resources, Purdue University, West Lafayette, Indiana

⁴Department of Geography, Texas A&M University, College Station, Texas

⁵U.S. Geological Survey, Boulder, Colorado

⁶U.S. Geological Survey, Lawrenceville, New Jersey

⁷College of Earth, Ocean, and Atmospheric Sciences, Oregon State University, Corvallis, Oregon

⁸Department of Geological Sciences, University of Alabama, Tuscaloosa, Alabama

⁹Departments of Marine and Environmental Sciences, Civil and Environmental Engineering, and Chemistry and Chemical Biology, Northeastern University, Boston, Massachusetts

Correspondence

Jacob D. Hosen, 195 Marsteller Street West Lafayette, IN 47906.

Email: jhosen@purdue.edu

Present address

Brett A. Poulin, Department of Environmental Toxicology, University of California Davis, Davis, CA, USA.

Funding information

Division of Environmental Biology, Grant/Award Number: 1457549; National Science Foundation Program Grants from Macrosystems, Grant/Award Numbers: 1442140, 1340749; 1824613

Abstract

Most terrestrial allochthonous organic matter enters river networks through headwater streams during high flow events. In headwaters, allochthonous inputs are substantial and variable, but become less important in streams and rivers with larger watersheds. As allochthonous dissolved organic matter (DOM) moves downstream, the proportion of less aromatic organic matter with autochthonous characteristics increases. How environmental factors converge to control this transformation of DOM at a continental scale is less certain. We hypothesized that the amount of time water has spent travelling through surface waters of inland systems (streams, rivers, lakes, and reservoirs) is correlated to DOM composition. To test this hypothesis, we used established river network scaling relationships to predict relative river network flow-weighted travel time (FWTT) of water for 60 stream and river sites across the contiguous United States (3090 discrete samples over 10 water years). We estimated lentic contribution to travel times with upstream in-network lake and reservoir volume. DOM composition was quantified using ultraviolet and visible absorption and fluorescence spectroscopy. A combination of FWTT and lake and reservoir volume was the best overall predictor of DOM composition among models that also incorporated discharge, specific discharge, watershed area, and upstream channel length. DOM spectral slope ratio ($R^2 = 0.77$) and Freshness Index ($R^2 = 0.78$) increased and specific ultraviolet absorbance at 254 nm ($R^2 = 0.68$) and Humification Index ($R^2 = 0.44$) decreased across sites as a function of FWTT and upstream lake volume. This indicates autochthonous-like DOM becomes continually more dominant in waters with greater FWTT. We assert that river FWTT can be used as a metric of the continuum of DOM composition from headwaters to rivers. The nature of the changes to DOM composition detected suggest this continuum is driven by a combination of photo-oxidation, biological processes, hydrologically varying terrestrial subsidies, and aged groundwater inputs.

KEYWORDS

biogeochemistry, dissolved organic matter, hydrology, limnology, travel time

1 | INTRODUCTION

Dissolved organic matter (DOM) is an important variable in freshwaters, acting as a fundamental heterotrophic energy source to food webs (Bernhardt et al., 2003; Hall & Meyer, 1998) and influencing the physicochemical environment (Kaplan & Cory, 2016). Yet, how ecosystem processes combine to form the DOM continuum of inland waters (Massicotte et al., 2017; Mosher et al., 2015; Vannote et al., 1980) remains a central knowledge gap for understanding inland water carbon cycling (Bernhardt et al., 2018; Kothawala et al., 2020; Palmer & Ruhi, 2019). Thus, identifying the factors linked to DOM, which represents half the flux of organic matter in freshwaters (Li et al., 2017), is necessary to inform the understanding of ecosystem processes that take place in individual lakes and rivers, as well as the global carbon cycle.

Freshwater DOM is often placed into two groups: allochthonous DOM that is fixed in terrestrial ecosystems and transported to aquatic environments and autochthonous DOM fixed by autotrophs within freshwaters (Kaplan & Cory, 2016). Allochthonous DOM is typically of higher apparent molecular weight, composed of more aromatic compounds that are often of less recent biological origin than autochthonous-like organic matter (Inamdar et al., 2013; Lynch et al., 2019), and compositionally resembles DOM found in terrestrial pore water (Fellman et al., 2009). Autochthonous-like DOM generally has a lower apparent molecular weight and higher microbial bioavailability than allochthonous DOM (Boyer et al., 2006; Hosen et al., 2014; Wünsch et al., 2018). Yet, freshwater DOM is a complex and heterogeneous mixture (Dittmar & Stubbins, 2014) and DOM source and molecular composition do not necessarily coincide (Inamdar et al., 2013). This is partly due to processing of terrestrial allochthonous DOM in streams and rivers, groundwater flowpaths and watershed networks by mineral sorption, bacterial uptake, and photo-oxidation (Koenig et al., 2019; Lynch et al., 2019; Tranvik & Bertilsson, 2008). Interestingly this processing of terrestrial DOM reduces the amount of DOM, but can leave behind material that compositionally resembles autochthonous DOM (Kaplan & Cory, 2016; Repeta, 2015).

Hydrology influences delivery of terrestrial DOM to inland waters. DOM concentrations generally increase with increasing discharge (Zarnetske et al., 2018) as allochthonous, terrestrial organic matter is flushed from organic-rich surficial soils and wetlands into waterways (Aitkenhead & McDowell, 2000; Boyle et al., 2009; Raymond & Saiers, 2010). Notably, during high flow events, fluvial DOM composition becomes more terrestrial (Hornberger et al., 1994; Raymond et al., 2016; Raymond & Saiers, 2010). In contrast, shifts from shallow upland flowpaths to greater groundwater contributions at low flow are accompanied by lower DOM concentrations that have less terrigenous signatures (Hosen et al., 2018; Inamdar et al., 2011). High flow events shorten fluvial travel times, leading to the “shunt” of DOM through the networks due to a processing time limitation (Raymond et al., 2016; Wollheim et al., 2018). Thus, although watershed geology, climate, and land use influence the composition of DOM entering waterways from watersheds, the terrigenous DOM

proportion generally increases with increasing discharge (Shultz et al., 2018; Wagner et al., 2019) and decreasing river travel time (Lynch et al., 2019).

Hydrology influences autochthonous production via channel depth and water clarity. Riverine water clarity increases during low flow/long travel time conditions due to lower levels of highly chromophoric allochthonous organic matter (Hensley et al., 2019) and particulates (Hosen et al., 2019). Increased light availability during low flow conditions favours increased aquatic photosynthesis (Hall et al., 2015; Hosen et al., 2019). Greater travel time during low flows allows more time for photosynthetic communities to develop biomass (Glibert et al., 2014; Paerl et al., 1998; Vannote et al., 1980). Productive algae release labile photosynthetic products, including sugars and proteins that have low apparent molecular weight and aromatic content, forming distinct compositional signatures (Aluwihare & Repeta, 1999; Bertilsson & Jones Jr, 2002; Hosen et al., 2021; T. Zhang & Wang, 2017).

Factors promoting production of autochthonous-like DOM during low flows also favour DOM processing via photo-oxidation and secondary production. Allochthonous organic matter travelling through river networks is continually degraded by photo-oxidation and biological activity (Catalán et al., 2016; Massicotte et al., 2017). Sunlight breaks aromatic rings and produces hydroxyl radicals, resulting in smaller DOM compounds that may have increased lability (Moran & Zepp, 1997; Tranvik & Bertilsson, 2008) and biological processes convert allochthonous DOM to biomass that is re-released as more autochthonous-like compounds (Hansen et al., 2016; Kamjunke et al., 2020; Lynch et al., 2019), which can include accumulation of proteins with increasing flow-weighted travel time (FWTT) of surface water within a river network (Peter et al., 2020). Lateral allochthonous inputs vary across ecosystems, but allochthonous inputs are greatest in headwaters and decrease in downstream rivers (Creed et al., 2015). Thus, as discharge decreases and the average travel time of surface water increases, greater light exposure and greater processing time lead to increased biological and photo-oxidative transformation (Lynch et al., 2019; Peter et al., 2020).

The relative contribution of aged groundwater to streamflow generally increases as river flow decreases, though the contribution of deep groundwater to surface flow is highly spatially variable (Poulsen et al., 2015). High groundwater storage time enhances DOM processing and sorption to mineral surfaces, and therefore groundwater generally carries low concentrations of DOM that lacks terrigenous optical and chemical markers and instead appears autochthonous-like (Kulkarni et al., 2017; O'Donnell et al., 2012). Thus, groundwater may add to the autochthonous-like signal of DOM observed with low flows and high water travel times (Hansen et al., 2016; Helms et al., 2014; Morling et al., 2017).

Major factors controlling DOM composition—contribution of terrestrial OM, rates of primary production, percent groundwater, and rates of processing—are all strongly related to flow and align so that high flows and associated fast travel times should carry more allochthonous terrestrial DOM and low flows should have DOM of autochthonous and autochthonous-like material. Studies of individual

systems indicate that riverine DOM composition can change drastically when it is transported through lakes or reservoirs (Maranger et al., 2018; Morling et al., 2017). Longer travel time through river networks due to travel through lakes and reservoirs also results in a transition of allochthonous to autochthonous DOM (Kellerman et al., 2015; King et al., 2019).

The importance of water travel time—that is, the average time that a drop of water has spent within a river network—is often discussed, but is difficult to estimate directly without tracers (Kirchner, 2019). One can use hydrogeomorphic scaling relationships to estimate relative variability in river or stream reach travel times (Allen & Pavelsky, 2018; Hay, 2019; Leopold & Maddock, 1953; Strahler, 1952; Worrall et al., 2014). Scaling relationships can be estimated using U.S. Geological Survey (USGS) river network hydrology records (U.S. Geological Survey, 2016) and stream, river, lake, and reservoir data from the National Hydrography Dataset (NHD) Plus (U.S. Geological Survey; McKay et al., 2012).

We applied river network scaling principles to quantify how the DOM continuum transitions from headwaters to major rivers of the United States. Specifically, we tested if DOM composition was consistently correlated with river network FWTT across the contiguous United States (CONUS). Thus, we (1) developed a model of relative river FWTT of water for streams and rivers included in the NHDPlus flow network; (2) estimated directly connected lake and reservoir volume for stream and river sites; and (3) assessed the correlation between FWTT and upstream lake and reservoir volume on composition of DOM quantified using ultraviolet–visible (UV–Vis) absorbance and fluorescence spectroscopy at 60 stream and river sites with watersheds of varying size located across CONUS.

2 | METHODS

2.1 | General approach

Here, we estimated FWTT for sites across CONUS by calculating the relationship between flow percentile and velocity for each stream order of each basin (see Figure S1 in Data S1 for workflow). For each stream reach, a random velocity and area were assigned given the mean and standard deviation of these values for a given flow percentile, stream order, and basin. Based on stream reach length and mean velocity, travel time for each stream reach upstream of a given point was calculated using NHDPlus flow maps. Muskingum–Cunge flow routing (Garbrecht & Brunner, 1991) was applied to determine the river water FWTT based on the relative amount of water coming from different tributaries (making the estimate flow-weighted). This approach was then replicated 1000 times for each site in order to obtain an estimate of model error (Figure S1 in Data S1). Based on the relationship between flow percentile and FWTT for a given stream site, we then assigned FWTT values for each DOM composition sample included in our analysis. We then assessed the relationship between FWTT of water within a river network and DOM composition and DOC concentrations of collected samples.

2.2 | Study sites

Water samples were collected from 60 sites in 14 basins ($n = 3090$) across CONUS (Table 1; Figure 1). Samples from 29 of these sites were collected as part of the USGS National Water Quality Network (NWQN) from 2008 through 2017 (Breitmeyer et al., 2019). Samples from 15 sites in the Connecticut River basin were collected from 2015 through 2017 (Hosen et al., 2019; Wagner et al., 2019). Samples from 11 sites in Maryland were collected from 2011 through 2013 (Hosen et al., 2014, 2017). Samples from seven sites studied as part of the National Science Foundation (NSF) Critical Zone Observatory (CZO) program were collected from 2009 through 2013 (Burns et al., 2016; Miller et al., 2016). Samples from one site, Mayfield Creek in the Mobile River basin, were collected from 2015 through 2016 (Shang, 2019). Sites were also grouped into five CONUS climatological regions (Midwest, Northwest, Northwest, South, Southwest) following Bukovsky (2011) and Prein et al. (2016).

2.3 | Sample collection

Connecticut River Basin Study. For Connecticut River basin samples—identified as “PulseShunt” in Table 1—water samples were filtered in the field through 0.2 μm polyethersulfone (PES) filters (Waters USA Inc.; Peshatin, Washington, USA). Samples were transported to the laboratory on ice and stored at 4°C until processing. Baseflow samples were collected at least monthly, and stormflow samples were collected seasonally. *USGS NWQN Study.* Samples collected for the USGS NWQN program (Table 1) were filtered in the field to 0.45 μm through Versapor filters (Pall Corporation; Port Washington, New York, USA) and stored at 4–6°C until analysis (Breitmeyer et al., 2019). Samples were collected following a pre-determined schedule. Thus, sampling captures a random sampling of flow conditions. *CZO Study.* Samples collected for the CZO study (Table 1) were stored on ice, filtered in the laboratory to 0.7 μm using pre-combusted Whatman GF/F filters, and the filtrate was stored at 4°C until analysis. Samples were collected approximately monthly during baseflow conditions (Miller et al., 2016). *Maryland Study.* Samples collected for the Maryland study were filtered in the field to 0.7 μm using pre-combusted Whatman GF/F filters (GE Healthcare, Chicago, Illinois, USA), and filtrate was stored at 4°C until analysis (Hosen et al., 2014). Baseflow samples were collected at least monthly, and stormflow samples were collected seasonally. *Mayfield Study.* All water samples were transported on ice and filtered through 0.2 μm PES filters. The filtrates were stored in pre-cleaned polycarbonate bottles at –20°C in the dark for the analysis of DOC and at 4°C in the dark for the analysis of DOM optical measurements. Samples were collected biweekly including baseflow and random stormflow conditions (Shang, 2019).

2.4 | DOM composition

UV–Vis and fluorescence protocols followed standard practice including blank subtraction. Fluorescence data were corrected for inner-filter effects and Raman-normalized (Cory et al., 2010).

TABLE 1 Information on study sites including the USGS station ID (if available), station name (USGS or other), latitude, longitude, Strahler stream order using NHDPlus classification, watershed area in km², in-network upstream lake and reservoir volume (km³), in-network lake and reservoir volume (km³) within study reach or immediate upstream tributaries, number of samples collected (n)

USGS ID	Station name	Basin	Study	Latitude	Longitude	Stream order	Watershed area (km ²)	Upstream lake volume (km ³)	Immediate upstream lake volume (km ³)	n
-	Gordon Gulch	Mississippi	CZO	40.012	-105.47	1	2.60	0	0	45
-	Mayfield Creek	Mobile	Mayfield	32.960	-87.408	2	1430	0	0	43
-	Parkers F8	Chesapeake Bay	Maryland	38.548	-76.542	1	0.124	0	0	6
-	Parkers F1	Chesapeake Bay	Maryland	38.548	-76.541	1	0.117	0	0	7
-	Parkers F6	Chesapeake Bay	Maryland	38.549	-76.543	2	0.214	0	0	7
-	Parkers F9	Chesapeake Bay	Maryland	38.550	-76.542	1	0.0524	0	0	8
-	Parkers F2	Chesapeake Bay	Maryland	38.551	-76.542	1	0.0419	0	0	8
-	Parkers F10	Chesapeake Bay	Maryland	38.550	-76.544	1	0.0728	0	0	8
-	Parkers F3	Chesapeake Bay	Maryland	38.550	-76.544	1	0.0697	0	0	8
01133000	E. Branch Passumpsic River Nr East Haven, VT	Connecticut	PulseShunt	44.634	-71.898	3	139.34	9.43x10 ⁻³	0	49
01134500	Moose River at Victory, VT	Connecticut	PulseShunt	44.512	-71.837	3	194.77	0.000242	0.000242	46
01135100	Pope Brook Trib (W-9), Nr North Danville, VT	Connecticut	PulseShunt	44.491	-72.162	1	0.470	0	0	80
01135150	Pope Brook (Site W-3) Near North Danville, VT	Connecticut	PulseShunt	44.476	-72.125	1	8.42	0	0	117
01135300	Sleepers River (Site W-5) Near St. Johnsbury, VT	Connecticut	PulseShunt	44.435	-72.038	3	111.1	0	0	84
01135500	Passumpsic River at Passumpsic, VT	Connecticut	PulseShunt	44.366	-72.039	4	1129	0.0135	0	94
01151500	Ottaquechee River at North Hartland, VT	Connecticut	PulseShunt	43.603	-72.355	4	572.4	0.00981	0.00352	6
01152500	Sugar River at West Claremont, NH	Connecticut	PulseShunt	43.488	-72.362	5	696.7	0.293	0.250	8
01177000	Chicopee River at Indian Orchard, MA	Connecticut	PulseShunt	42.161	-72.514	5	1785	0.180	0.116	6
01184000	Connecticut River at Thompsonville, CT	Connecticut	PulseShunt	41.987	-72.605	6	25019.3	3.47	0.658	51
01186500	Still River at Robertsville, CT	Connecticut	PulseShunt	41.968	-73.033	4	220.15	0.0110	0	185
01187300	Hubbard River Near West Hartland, CT	Connecticut	PulseShunt	42.038	-72.939	3	51.54	0	0	43
01187800	Nepaug R Nr Nepaug, CT	Connecticut	PulseShunt	41.821	-72.970	3	60.86	1.11x10 ⁻⁴	5.19x10 ⁻⁶	39
01187830	Phelps Brook at Mill Dam Road Nr Collinsville	Connecticut	PulseShunt	41.800	-72.965	1	6.99	0	0	76
01188000	Bunnell Brook Near Burlington, CT	Connecticut	PulseShunt	41.786	-72.965	1	10.62	0	0	149
01188090	Farmington River at Unionville, CT	Connecticut	PulseShunt	41.756	-72.887	5	979.02	0.298	0.244	41

TABLE 1 (Continued)

USGS ID	Station name	Basin	Study	Latitude	Longitude	Stream order	Watershed area (km ²)	Upstream lake volume (km ³)	Immediate upstream lake volume (km ³)	n
01189995	Farmington River at Tariffville, CT	Connecticut	PulseShunt	41.908	-72.759	5	1494.42	0.301	0.245	228
01372043	Hudson River Below Poughkeepsie NY	Hudson	NWQN	41.651	-73.945	7	30406.46	1.65	0.327	48
01463500	Delaware River at Trenton NJ	Delaware	NWQN	40.222	-74.778	6	17560.12	3.62x10 ⁻⁶	0	51
01479000	White Clay Creek Near Newark, Delaware	Susquehanna	CZO	39.699	-75.675	4	230.7679	0.000308	0	8
01578310	Susquehanna River at Conowingo, MD	Susquehanna	NWQN	39.658	-76.174	7	70188.73	2.74	1.35	43
01646580	Potomac River at Chain Bridge, Washington, DC	Potomac	NWQN	38.930	-77.117	7	29966.18	0.0986	1.57x10 ⁻⁴	103
02226160	Altamaha River Near Everett City, GA	Altamaha	NWQN	31.427	-81.605	7	36259.86	0.155	0.09254	102
02359170	Apalachicola River Nr Sumatra, FL	Apalachicola	NWQN	29.949	-85.015	8	49727.77	3.07	1.05	68
02470500	Mobile River at Mt Vernon AL	Mobile	NWQN	31.087	-87.977	8	111025.1	3.93	0.618	26
03303280	Ohio River at Cannelton Dam at Cannelton, IN	Mississippi	NWQN	37.900	-86.706	8	251228.85	5.13	0.107	49
03374100	White River at Hazleton, IN	Mississippi	NWQN	38.490	-87.55	7	29279.82	0.763	1.12x10 ⁻⁵	59
03378500	Wabash River at New Harmony, IM	Mississippi	NWQN	38.132	-87.94	8	75715.71	1.30	1.24x10 ⁻⁴	45
03612600	Ohio River at Olmsted, IL	Mississippi	NWQN	37.179	-89.058	9	525767.59	21.6	3.12	30
05420500	Mississippi River at Clinton, IA	Mississippi	NWQN	41.781	-90.252	8	221702.98	31.1	2.94	32
05465500	Iowa River at Wapello, IA	Mississippi	NWQN	41.178	-91.182	7	32374.85	0.280	0.101	32
05490500	Des Moines River at Keosauqua, IA	Mississippi	NWQN	40.728	-91.96	7	36358.25	0.852	0.502	31
05586100	Illinois River at Valley City, IL	Mississippi	NWQN	39.703	-90.645	8	69264.1	1.34	0.451	46
06610000	Missouri River at Omaha, NE	Mississippi	NWQN	41.259	-95.923	9	836048.16	79.0	35.6	48
06805500	Platte River at Louisville, NE	Mississippi	NWQN	41.015	-96.158	8	221107.28	4.65	2.95	39
07373420	Mississippi River Near St. Francisville, LA	Mississippi	NWQN	30.758	-91.395	10	2135617.69	162	10.7	54
07374000	Mississippi River at Baton Rouge, LA	Mississippi	NWQN	30.446	-91.192	10	2915836.64	162	10.7	46
07374525	Mississippi River at Belle Chasse, LA	Mississippi	NWQN	29.857	-89.978	10	2926688.7	162	10.7	85
07381495	Atchafalaya River at Melville, LA	Mississippi	NWQN	30.691	-91.736	10	241687.51	170	1.79	82
08116650	Brazos Rv Nr Rosharon, TX	Brazos	NWQN	29.350	-95.582	7	117427.47	2.25	1.15	59
09522000	Colorado River at Nib, Above Morelos Dam, AZ	Colorado	NWQN	32.719	-114.719	9	638950.53	50.5	25.9	44
11303500	San Joaquin R Nr Vernalis CA	San Joaquin	NWQN	37.676	-121.266	7	35065.87	3.54	0.644	91
11447650	Sacramento R at Freeport CA	Sacramento	NWQN	38.456	-121.501	7	61316.68	9.44	4.74	48
14246900	Columbia R at Pt Westward Nr Quincy OR	Columbia	NWQN	46.181	-123.183	9	665368.43	69.0	19.8	82
-	Shale Hills	Susquehanna	CZO	40.700	-77.889	1	0.99	0	0	29
-	P301 - Southern Sierras CZO	San Joaquin	CZO	37.063	-119.205	1	99	0	0	12

(Continues)

TABLE 1 (Continued)

USGS ID	Station name	Basin	Study	Latitude	Longitude	Stream order	Watershed area (km ²)	Upstream lake volume (km ³)	Immediate upstream lake volume (km ³)	n
-	Parkers F4	Chesapeake Bay	Maryland	38.512	-76.523	1	0.02855	0	0	6
-	Parkers F11	Chesapeake Bay	Maryland	38.511	-76.522	1	0.0713179	0	0	7
-	Parkers F7	Chesapeake Bay	Maryland	38.512	-76.524	2	0.167499	0	0	7
-	White Clay Creek at Swrc Pumphouse	Susquehanna	CZO	39.861	-75.784	2	7.018868	3.62x10 ⁻⁶	3.62 x10 ⁻⁶	97
01193050	Connecticut R. at Middle Haddam, Ct	Connecticut	PulseShunt	41.542	-72.554	6	2822312.1	3.798	0.662	43

Note: Data were compiled from numerous studies. The relevant studies for each site are provided in the table. Studies include the Critical Zone Observatory (CZO) study (Miller et al., 2016), the Mayfield study, Maryland Coastal Plain streams (Febria et al., 2015; Hosen et al., 2014, 2017), the PulseShunt study (Hosen et al., 2019; Wagner et al., 2019), the National Water Quality Network (NWQN) dataset (Breitmeyer et al., 2019), and the Mayfield Creek Study (Shang, 2019).

For Connecticut River samples, UV-Vis absorption spectra and fluorescence excitation-emission matrices (EEMs) were collected using a Horiba Aqualog spectrofluorometer. Spectra were measured on samples in a quartz cuvette with a 1 cm pathlength. UV-Vis absorbance from 200–800 nm was collected at 1 nm increments with an integration time of 1 s. EEMs were collected at excitation wavelengths of 240 to 800 nm at 3 nm increments and fluorescence emission from 247.808 to 828.528 nm at 2.06 nm increments using 4 CCD pixel integration. Raman scattering area was determined using Type I (18.2 M Ω -cm) water from a Milli-Q Advantage A-10 water purification system, integrating fluorescence from 247.808 to 828.528 nm emission at an excitation wavelength of 350 nm with an integration time of 10 s (Stedmon et al., 2003). Spectra of at least 4 water blanks were collected during each analytical run.

The USGS NWQN study measured UV-Vis absorbance using an Agilent HP8453 spectrophotometer, fluorescence using a Horiba Fluoromax-3 fluorometer, and dissolved organic carbon (DOC) concentrations using an OI700 carbon analyser. The CZO study measured UV-Vis absorption using a Shimadzu UV-1800 spectrophotometer, fluorescence using a Horiba Fluoromax-4 spectrofluorometer, and DOC with a Shimadzu TOC-V_{CPH} analyser (Miller et al., 2016). The Maryland study measured absorption using a Thermo Scientific Evolution 60 spectrophotometer, fluorescence using a Horiba Fluoromax-4 spectrofluorometer, and DOC with a Shimadzu TOC-V_{CPH} analyser (Hosen et al., 2014). The Mayfield study measured absorption using a Shimadzu UV-1800 spectrophotometer, fluorescence using a Horiba FluoroMax-3 spectrofluorometer, and DOC using a Shimadzu TOC-V_{CPH} analyser (Shang et al., 2018).

Spectral slope ratio (S_R) and specific ultraviolet absorbance at 254 nm (SUVA₂₅₄), metrics of DOM composition obtained from UV-Vis spectra, were calculated for most sites. S_R is the ratio of log-transformed absorbance slopes between 275–295 nm and 350–400 nm (Helms et al., 2008). SUVA₂₅₄ is the decadic absorption coefficient at 254 nm divided by the DOC concentration and is presented in units of L mg-C m⁻¹ (Weishaar et al., 2003). Freshness index is the ratio of fluorescence emission at 380 nm divided by the maximum emission intensity from 420 to 435 nm at excitation wavelength of 310 nm (Parlanti et al., 2000, p. 200; Wilson & Xenopoulos, 2009). FI is the ratio of fluorescence emission at 470 and 520 nm at excitation 370 nm (Cory et al., 2010; McKnight et al., 2001). HIX is the summation of fluorescence emissions at 435–480 nm divided by the sum of fluorescence emission at 300–345 nm, at excitation 254 nm (Ohno, 2002).

To confirm that the results of this study are not contingent on analytical differences between laboratories, we tested whether relationships reported were significantly altered by potential study effects tied to individual instruments. To do this, we incorporated *Study* (NWQN, CZO, Maryland, PulseShunt, and Mayfield) as a categorical covariate in our mixed effects models (see *Bivariate Statistical Analysis* below for methods; Figure S2 in Data S1). Incorporating *Study* as a factor did not improve the overall fit of the models tested and was removed. To investigate the influence of filter type used in this study (GF/F vs. 0.2 μ m PES), we compared the results from 14 matched

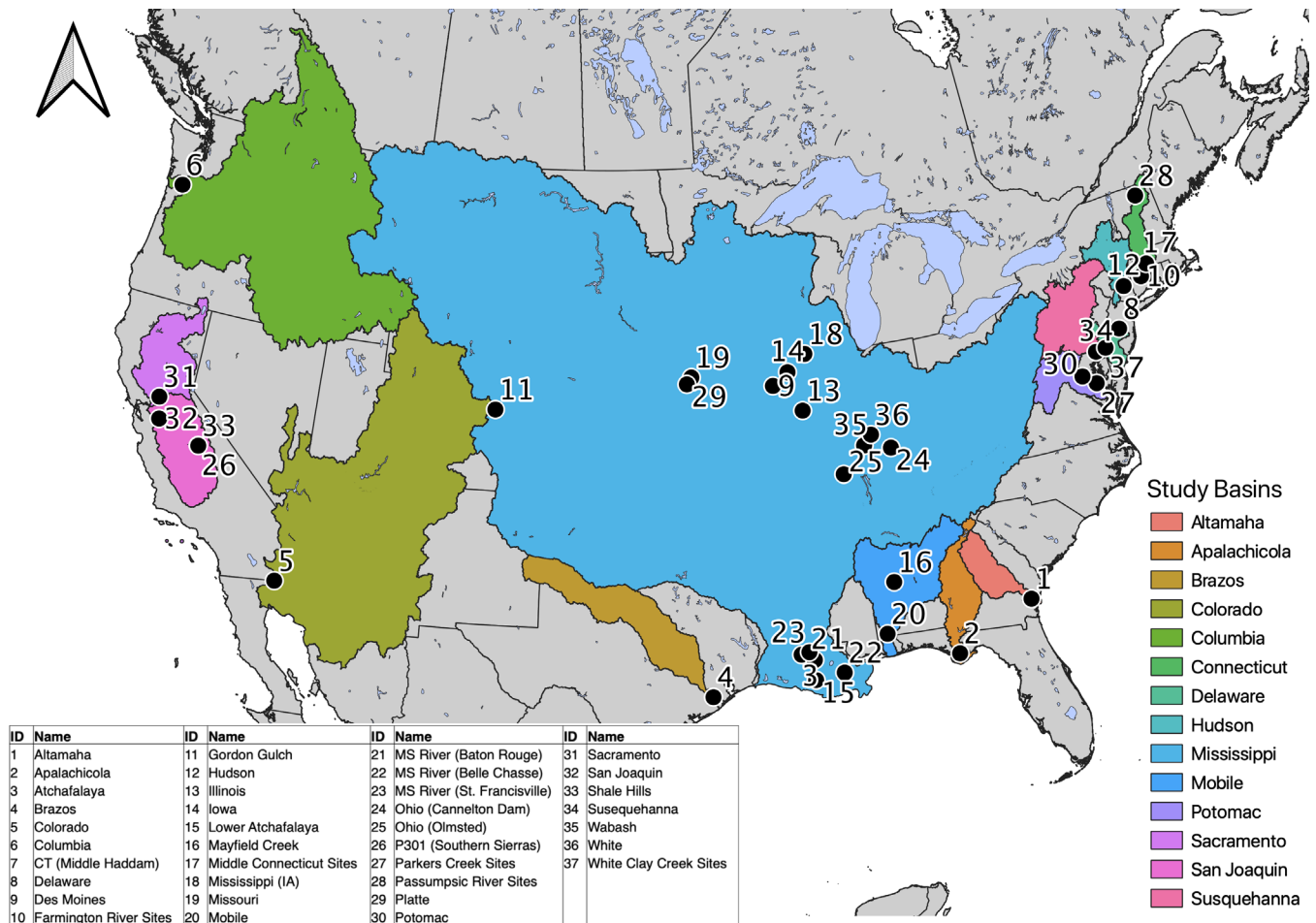


FIGURE 1 A map of the 60 study sites within CONUS. The 14 different river basins, with the addition of sites located along the Chesapeake Bay, are distinguished by colour. Individual sites are identified with numbers. If multiple sites were too close to distinguish individually, these sites were identified by a single marker. This was the case for the Farmington River sites (10; Still River, Hubbard River, Nepaug River, Phelps Brook, Bunnell Brook, Farmington River at Tariffville, Farmington River at Unionville), the Middle Connecticut Sites (21; Ottaquechee River, Sugar River, Chicopee River), the Parkers Creek Sites (27; Parkers F1, F2, F3, F4, F6, F7, F8, F9, F10, F11), the Passumpscic River Sites (28; E. Branch Passumpscic River, Moose River, Pope Brook Tributary W9, Pope Brook, Sleepers River, Passumpscic River) and the White Clay Creek Sites (37; White Clay Creek at SWRC Pumphouse and White Clay Creek near Newark). For more detailed site information see Table 1

samples collected as part of the Connecticut River study. We found that DOC concentrations ($R^2 = 0.99$), S_R ($R^2 = 0.76$), HIX ($R^2 = 0.94$), Freshness ($R^2 = 0.91$), FI ($R^2 = 0.86$), and $SUVA_{254}$ ($R^2 = 0.78$) were highly correlated between the two filter types in all cases ($ndf = 1$, $ddf = 13$, $p < 0.0001$; Table S2 in Data S1). This is consistent with research showing the vast majority of DOM is smaller than $0.2 \mu m$ (Wünsch et al., 2018). Thus, we argue that incorporating data from multiple studies did not impact our analysis.

2.5 | Travel time

We estimated flow-weighted river travel time across flow levels based on Muskingum-Cunge flow routing (Garbrecht & Brunner, 1991) as is done for the USGS National Hydrologic Model (Hay, 2019) and recently published work (Worrall et al., 2014). For each basin we accessed USGS hydrology data from the National Water Information

System (U.S. Geological Survey, 2016). We downloaded daily discharge for the study period (water years 2008–2018) and field-surveyed estimates of mean channel velocity and channel cross-sectional area (converted to m^2) for all gaged sites within a study basin. Given that hydraulic geometry has been shown to be consistent within a given stream order across individual basins (Allen, Pavelsky, et al., 2018) this approach was deemed appropriate. We identified upstream networks and USGS gage sites by subsetting NHDPlus (<http://www.horizon-systems.com/nhdplus/>) flowlines to include only features located above a given study reach using the connectivity information provided. We estimated hydrology (velocity, area, and discharge) for each upstream stream order using USGS data. Larger basins with sufficient numbers of USGS gaging stations were selected for sites where sufficient upstream data were not available. The basin from which hydrological data were drawn is indicated for each site in Table 1.

While USGS gage locations are sometimes located at unrepresentative positions within the river network, there are several

reasons why we elected to use these data. First, the scaling estimates that we generated do not deviate substantially from those established by Leopold and Maddock (1953) during surveys of rivers of the United States of America. The reason is due to at-many-stations hydrologic geometry (AMHG; Gleason & Smith, 2014), which shows that depth, width, velocity, and discharge geometry values are spatially invariant across stations in a river (Barber & Gleason, 2018). Thus, our hydraulic scaling estimates are robust to sampling location along a reach. We generated scaling relationships with contemporary data rather than using hydraulic scaling equations that were developed previously (Leopold & Maddock, 1953) because changes to climate patterns have changed hydrologic geometry in many basins (Dunne & Leopold, 1978). Instead, we have limited hydrologic analysis to hydrology data collected over the course of the study period (2008–2018). We apply 10 years of data to capture the full set of hydrologic conditions over the study period. Due to the availability of large amounts of data, we take a data-driven approach to estimate hydraulic geometry properties of stream networks. For regions or time periods lacking stream gage data, other methods to estimate hydraulic geometry, including emerging remote sensing techniques (Gleason et al., 2014), could also be used.

We computed flow-exceedance curves using the *hydroTSM* (Mauricio Zambrano-Bigiarini, 2017) package in R 3.6.0 (R Core Team, 2018) to estimate discharge percentiles over the study period (2008–2018). For ease of interpretation, increasing flow percentile numbers correspond to increasing flow. For each stream order in each basin, we determined the average and standard error for mean channel velocity and channel cross-sectional area at flow percentiles from 1 through 99 at 1-unit intervals. Plots of model results for study sites are available as Figure S8 in Data S1.

We combined the estimates of velocity and cross-sectional area across flow levels with the subsetted NHDPlus networks. For each flow percentile, we assigned a cross-sectional area and stream flow velocity to each NHDPlus reach based on the given flow percentile, stream order, and basin. The cross-sectional area and stream velocity values for each reach were randomly selected from a normal distribution with a mean and standard deviation for the appropriate flow percentile, stream order, and basin. Next, we obtained travel time for each reach by dividing reach length (supplied by NHDPlus) by the stream velocity. We obtained discharge for each reach by multiplying cross-sectional area by stream velocity. Lastly, we calculated FWTT for water in each reach, beginning at the top of each river network and following river network flowpaths. For each NHDPlus reach, cumulative FWTT was calculated as follows.

$$FWTT_i = \frac{l_i}{v_i} + \sum_{j=1}^{reaches} \frac{FWTT_j * Q_j}{\sum_j reaches Q_j} \quad (1)$$

$$Q_j = v_j * A_j \quad (2)$$

Here, i , indicates the reach for which cumulative FWTT ($FWTT_i$) is calculated using length (l_i) and velocity (v_i) of reach i . $FWTT_j$ from each upstream reach (j) is scaled by the relative amount of discharge from

each upstream reach (Q_j). Equation (1) was calculated for each reach within a given network, starting at the headwaters and continuing downstream to the reach that includes the sampling site for this study. The result of Equation (1) for that most downstream reach becomes the estimate of the FWTT for a given sampling location. For each flow percentile (1st to 99th) at each site, this process was completed 1000 times, using different random drawings of cross-sectional area (A_j) and velocity (v_j) for each reach on each replicate. To generate a final FWTT estimate for each site at a given flow percentile, we took the mean and 95% confidence interval of the 1000 replicate estimates.

2.6 | FWTT validation

The scale of this study means that tracers and other traditional methods of measuring water travel times were not feasible. Thus, we compared the present results to those of Allen, David et al. (2018). The results by Allen, David et al. (2018) were developed using a kinematic wave model to estimate river FWTT under bankfull conditions. The recurrence interval of bankfull conditions in rivers is variable, but generally lies between 1.2 and 1.5 years for rivers in the United States (Castro & Jackson, 2001; Simon et al., 2004). Thus, we compared the bankfull results from the existing study to the high flow level calculated here—99th percentile, which is a 1 in 100-day recurrence interval flow.

2.7 | Lakes and reservoirs

For each watershed, we determined the volume of lakes and reservoirs that were directly connected to the river network. We used the *v.overlay* function in Grass GIS 7.4.0 (GRASS Development Team, 2018) to identify lakes and reservoirs directly connected to river network flowlines. Attributes from the NHDPlus Waterbody shapefile were used for lake and reservoir locations and volumes. We identified upstream water bodies and used this information to determine the *total upstream* in-network lake volume for a given stream reach using characteristics for each water body provided by NHDPlus. We also calculated the volume of only lakes and reservoirs that were *immediately upstream* of the study site. Here we define *immediately upstream* as being within the study reach or directly connected tributary reaches of a lower order.

2.8 | Bivariate statistical analysis

We calculated repeated-measures mixed effects models with DOM composition metrics as the dependent variables and watershed and hydrological variables as independent variables. Models were computed using the *lme4* (Bates et al., 2015) and *lmerTest* (Kuznetsova et al., 2017) packages in R 3.6.0. For each DOM metric (S_R , $SUVA_{254}$, Freshness, FI, HIX), we tested a set of models using the following combinations of independent variables: (1) $\log_{10}(\tau)$, (2) $\log_{10}(\tau)$

+ LV_conn, (3) $\log_{10}(\tau)$ + LV_conn_imm, (4) $\log_{10}(Q)$, $\log_{10}(Q)$ + LV_conn, (5) $\log_{10}(Q)$ + LV_conn_imm, (6) $\log_{10}(SQ)$, $\log_{10}(SQ)$ + LV_conn, (7) $\log_{10}(SQ)$ + LV_conn_imm, $\log_{10}(WA)$, (8) $\log_{10}(WA)$ + LV_conn, (9) $\log_{10}(WA)$ + LV_conn_imm, (10) $\log_{10}(L_km)$, (11) $\log_{10}(L_km)$ + LV_conn, (12) $\log_{10}(L_km)$ + LV_conn_imm. Here $\log_{10}(\tau)$ is log-transformed FWTT (τ) in days, $\log_{10}(Q)$ is log-transformed water discharge (Q) in $m^3 s^{-1}$, $\log_{10}(SQ)$ is log-transformed specific discharge (SQ) in $m^2 s^{-1}$, $\log_{10}(WA)$ is log-transformed watershed area (WA) in hectares, and $\log_{10}(L_km)$ is the sum of upstream channel length according to NHDPlus. LV_conn is total water volume (m^3) of upstream lakes and reservoirs directly connected to the river network as determined from NHDPlus V2. LV_conn_imm is the total volume (m^3) of lakes and reservoirs immediately upstream of the sampling site directly connected to the river network (as described above). Models were tested for homoscedasticity and normal distribution of residuals.

Most models tested returned highly significant values ($p < 0.001$) due to large sample sizes. Thus, we used conditional Akaike Information Criterion (cAIC), which is appropriate for linear mixed effects model selection (Grevén & Kneib, 2010; Saefken et al., 2014) using the *cAIC4* package (Säfken et al., 2018) in R 3.6.0. Due to maximum likelihood estimation, traditional R^2 calculations cannot be estimated with mixed-effects. Marginal R^2 values provide information on the goodness of model fit across experimental units (sites), while conditional R^2 provides information on goodness of fit within experimental unit model fit (Nakagawa et al., 2017; Nakagawa & Schielzeth, 2013). Both were computed using the R *piecewiseSEM* package (Lefcheck, 2016).

We analyzed mean FWTT and DOM composition for each site included in the study (Table 1, Table S1 in Data S1). We compared each DOM composition metric to the set of predictor values selected by mixed effect model selection using *lm* in R. For models that were not unimodal, a quadratic polynomial model was adopted if model assumptions were met. Model fits were evaluated in R using second-order Akaike's Information Criterion (AICc; using the *MuMIn* package in R [Bartoń, 2018]), R^2 , and adjusted R^2 .

2.9 | Multivariate statistical analysis

We compared hydrology and DOM composition using co-inertia analysis in the R *ade4* package (Dray & Dufour, 2007). Co-inertia analysis compares multivariate datasets with the objective of finding the maximum shared variance between two discrete groups of variables (Doledec & Chessel, 1994; Dray et al., 2003). Here, we divided the dataset into two groups of variables. The first group was composed of variables related to hydrology—site FWTT, lake and reservoir volume, immediate upstream lake and reservoir volume, upstream channel length, and watershed area. The second group included metrics of DOM composition— S_R , freshness index, FI, $SUVA_{254}$, and HIX. First, principal component analysis (PCA) was computed on the two groups of variables then co-inertia analysis was used to estimate the relationship between the two PCA models. Similarity between the datasets is

measured with the RV coefficient, which varies between 0 and 1, with 1 indicating the greatest overall similarity between the two datasets.

3 | RESULTS

3.1 | FWTT scaling

Streamflow velocity (Figure S3a–c in Data S1), channel length (Figure S3d–f in Data S1), and resulting travel time for water within each stream order (Figure 3g–i in Data S1) varied across the 13 major basins of this study (Table 1). Streamflow velocity, channel length, and travel time increased with stream order (Figure S3 in Data S1). However, because length increased at a faster rate than velocity, mean travel time per stream order increased with increasing stream order (Figure S3g–i in Data S1) although travel time per km decreased with stream order (Figure S3j–l in Data S1). FWTT at 50th percentile flow for the 14 study basins ranged from 0.04 to 27.9 days (Table S1 in Data S1; Figure 2). Consistent with river network scaling relationships (Church & Mark, 1980; Leopold & Maddock, 1953), travel time at average flow was correlated with river order, upstream channel length, watershed area, and 50th percentile discharge of a site (Figure 2). The most consistent predictor of travel time was upstream channel length ($F_{(1,70)} = 583.3$; $R^2 = 0.907$; $p < 0.0001$). This relationship showed power scaling: $FWTT = 0.07888 * (StreamLength)^{0.42}$, where FWTT is in units of days and StreamLength is total upstream length in km of all upstream channels mapped as part of NHDPlus V2. We found agreement between previous estimates of flood wave travel time by Allen, David et al. (2018) and estimates of river network FWTT at 99th percentile flows in the present study ($F_{(1,34)} = 41.6$; $p < 0.0001$; $R^2 = 0.55$; Figure S4 in Data S1). While there was variability, the regression generated for the comparison was similar to a 1:1 line, $TravelTime[Allen] = 1.20 \times TravelTime[PresentStudy] - 0.20$.

Total upstream lake and reservoir volume increased gradually with river size before a strong increase with 9th and 10th order streams. This pattern was not repeated for immediate upstream lake and reservoir volume, where a small increase was found for 9th order streams before volume decreased in 10th order streams (Figure 2e,f). Immediate upstream lake and reservoir volume—which includes lakes and reservoirs in the upstream reach and all direct tributaries of that reach (see *Methods* section for details)—did not scale as consistently with stream order. Some relatively large rivers did not have any immediate upstream lake or reservoir surface volume including the Potomac River at Washington, DC and the Wabash River in Indiana (Table 1).

3.2 | FWTT and DOM composition

We evaluated the hydrologic links to DOM composition on both a sample-wise and site-wise basis. For the sample-based analysis, we compared whether river network FWTT, discharge, or specific discharge (calculated as discharge divided by watershed area) associated with a particular sample were better predictors of DOM composition.

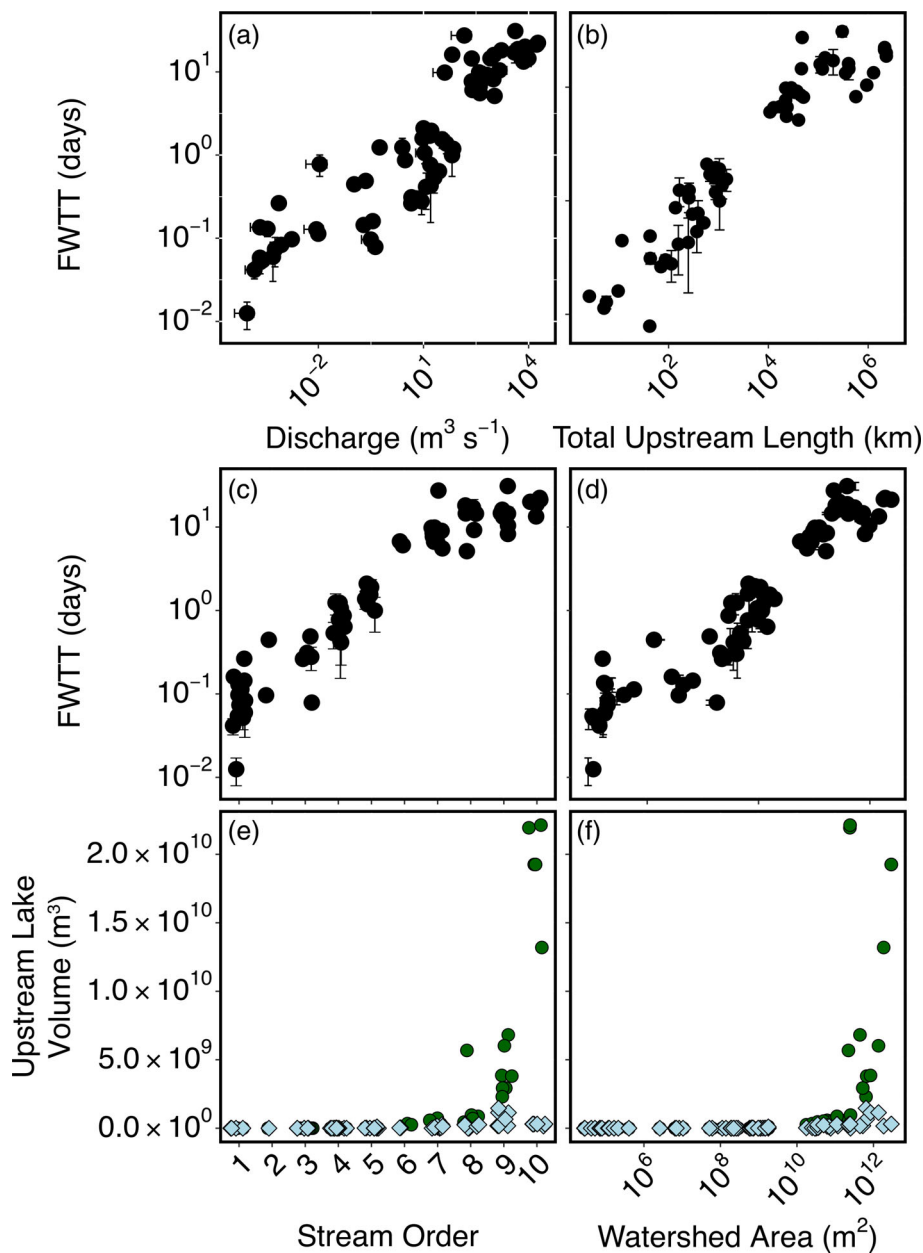


FIGURE 2 Site mean FWTT vs. discharge (a) and total upstream channel length (km) as determined from NHDPlus v2, (b) at 50th percentile flows. Plots of FWTT compared to stream order (c), and site watershed area (d) are included. Connected upstream lake volume (encompassing both lakes and reservoirs) as related to stream order (e) and watershed area (f) is plotted. In plots a–d, error bars present standard error of the mean for either discharge or FWTT. In plots e and f, green circles represent *total* upstream lake and reservoir surface area and blue diamonds represent *immediate upstream* lake and reservoir surface area. Here immediate upstream lakes are water bodies that are in the upstream reach and in tributaries directly connected to this reach

For the site-based analysis, we compared mean DOM composition at a site to mean values of FWTT, specific discharge, and discharge.

We found that estimates of FWTT were the best hydrologic predictors of DOM composition across all sites (Figures 3 and 4, Table 2, Table S3 in Data S1). We also found that a model incorporating both FWTT and the sum of in-network lake and reservoir volume in the river reach and upstream tributaries significantly improved DOM composition correlations. Immediate upstream lake and reservoir volume (encompassing connected lake and reservoir volume that was in the study reach or tributary reaches directly connected to the study reach) was a significantly better covariate for predicting S_R and Freshness Index than total upstream lake and reservoir volume for S_R and Freshness Index values (Figure 3; Table 2; Table S3 in Data S1).

FWTT was consistently a better predictor of S_R , Freshness Index, and $SUVA_{254}$ than other hydrologic variables tested (i.e., discharge,

specific discharge, watershed area, or upstream channel length; Table 2 and Table S3 in Data S1). In the case of S_R , using log-transformed FWTT as a predictor gave a marginal R^2 of 0.58, compared to 0.32, 0.20 and 0.13 for upstream channel length, discharge, and specific discharge, respectively. For S_R , a model incorporating log-transformed FWTT and immediate upstream lake and reservoir volume had the lowest cAIC value (Conditional $R^2 = 0.86$; Marginal $R^2 = 0.61$; Figure 4a; Figure S5a in Data S1; Table 2; Table S3 in Data S1). Site mean values of S_R and FWTT were also correlated ($R^2 = 0.77$; Figure 3b; Table 2). For the Freshness Index, models incorporating immediate upstream lake volume along with FWTT returned best fit among options evaluated for both the mixed effects (Figure 3a; Figure S5b in Data S1; Conditional $R^2 = 0.90$; Marginal $R^2 = 0.59$; Table 2) and linear regression of site mean values ($R^2 = 0.78$; Figure 3d; Table 2) analyses.

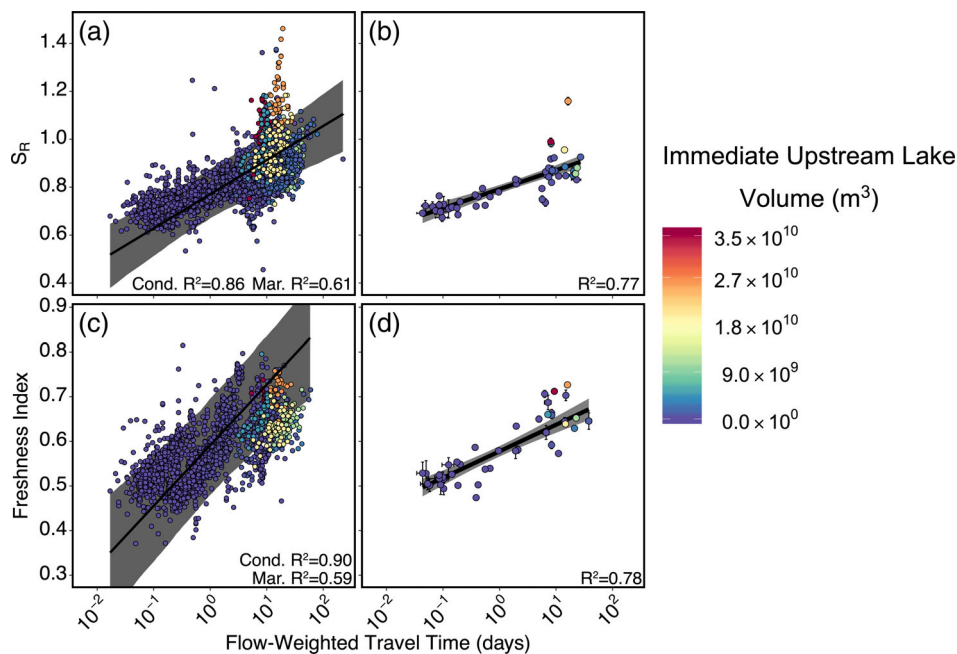


FIGURE 3 FWTT (in days) of a water sample was compared to DOM composition variables where immediate in-network upstream lake and reservoir volume (m^3) significantly improved the overall model fit according to cAIC statistics. Results for spectral slope ratio (S_R ; (a,b) and freshness index (c,d) are presented. The first column of plots (a,c), present results of the mixed effects model incorporating the estimate of the overall fit with associated 95% confidence band. Each point represents an individual sample. The second column of plots (b,d), present results using site mean values; each point represents the mean value of all samples for a site and the error bars represent standard error of the mean for each site, and lines represent results of linear regression models with associated 95% confidence bands. Each point is colour-coded according to the volume of in-network lakes and reservoirs immediately upstream of the sampling site

Aromatic and humic-like DOM fractions ($SUVA_{254}$, HIX) consistently decreased with increasing FWTT and lake and reservoir volume. For $SUVA_{254}$, a model incorporating FWTT and in-network upstream lake area returned the lowest AICc value (Conditional $R^2 = 0.44$; Marginal $R^2 = 0.66$; Figure 4a; Figure S5c in Data S1; Table 2). For site mean $SUVA_{254}$ values, a model that included log-transformed FWTT and total connected lake volume was the best fit ($R^2 = 0.68$; Figure 4b; Table 2). In the case of humification index ($\log_{10}[\text{HIX}]$), model results were similar to $SUVA_{254}$ (Marginal $R^2 = 0.29$; Conditional $R^2 = 0.68$; Figure 4c; Figure S5d in Data S1; Table 2; Table S3 in Data S1). Site-wise mean HIX values indicated that log-transformed FWTT combined with total upstream lake area were correlated to HIX across sites ($R^2 = 0.44$; Figure 4d; Table 2). FI was best predicted by log-transformed FWTT and total upstream connected lake and reservoir volume (Marginal $R^2 = 0.33$; Conditional $R^2 = 0.94$; Figure 4e; Figure S5e in Data S1). To fit model assumptions, models involving site means of FI required predictor values included as quadratics for analysis of site-wise mean values. Unlike other DOM composition metrics, the relationship between FWTT and FI was not monotonic. Thus, the quadratic predicting FI including log-transformed FWTT, log-transformed FWTT squared, and immediate upstream lake volume ($R^2 = 0.43$; Figure 4f; Table 2) was the best-fitting model considered.

In contrast to DOM composition, DOC concentration and DOC watershed yield were not strongly correlated to FWTT or other hydrological variables evaluated (Figure S6 in Data S1). Instead,

among the variables evaluated DOC concentration and yield at sites were most strongly correlated to discharge (Table S4 in Data S1). Across sites, DOC concentration was explained best by watershed area and immediate upstream lake volume ($R^2 = 0.25$, Table S6 in Data S1). The relationship between DOC concentration and FWTT and immediate upstream lake volume was not as strong ($R^2 = 0.22$). DOC yield across sites was not significantly correlated to any of the metrics evaluated (Table S5 in Data S1).

Plots are presented with samples plotted according to the basin (Figure S7a,c,e,g,i in Data S1) and region of CONUS (Figure S7b,d,f,h,j in Data S1) of the sample sites. Statistical analysis showed that adding either basin or region marginally improved model fit in some cases (Table S6 in Data S1). Yet, for many levels of basin and region only one site was sampled for this study (Tables S7 and S8 in Data S1) and the range of FWTT values are limited (Figure S7 in Data S1). Thus, further data are needed to better test regional differences.

3.3 | Hydrology and DOM composition: Multivariate analysis

We used co-inertia analysis to compare river network hydrology variables to DOM composition (Figure 5). We found that a substantial proportion of variance was explained between these two groups ($RV = 0.40$). We present mean projected co-inertia scaling values for

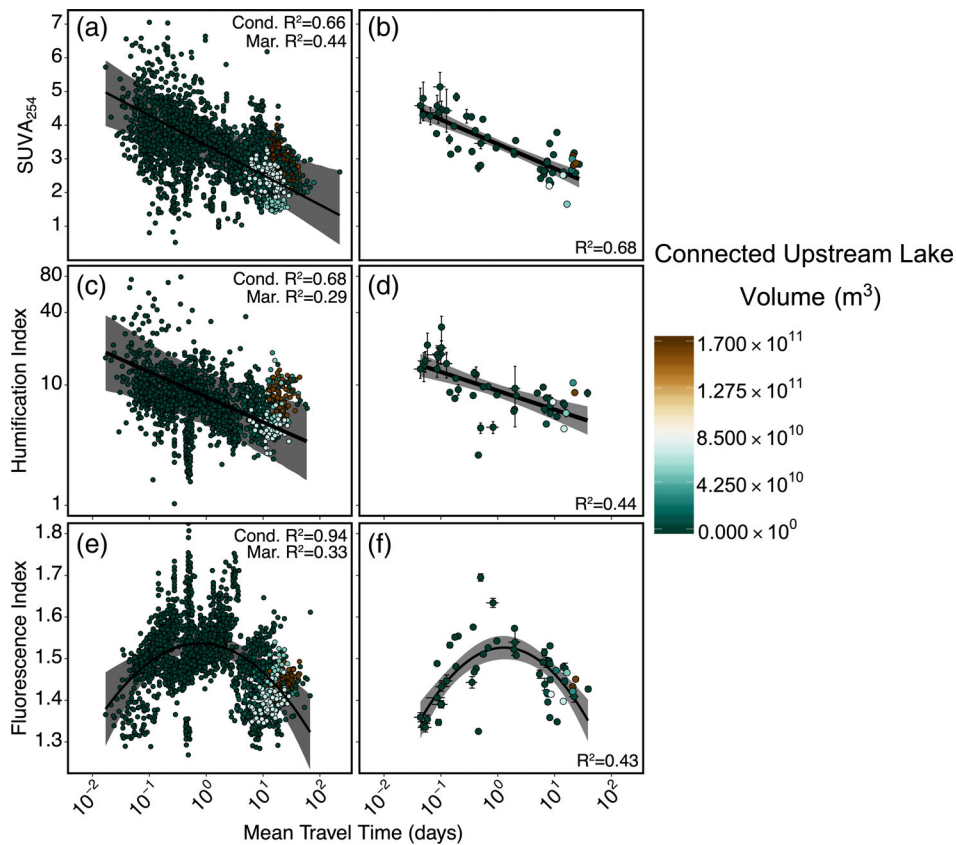


FIGURE 4 FWTT (in days) of a water sample was compared to DOM composition variables where total in-network upstream lake and reservoir volume (m^3) significantly improved the overall model fit according to cAIC statistics. Results for specific ultraviolet absorbance at 254 nm (SUVA_{254} ; (a,b), humification index (c, d), and fluorescence index (e,f) are presented. The first column of plots (a,c,e), present results of the mixed effects model incorporating the estimate of the overall fit with associated 95% confidence band. Each point represents an individual sample. The second column of plots (b,d,f), present results using site mean values; each point represents the mean value of all samples for a site, the error bars represent standard error of the mean for each site, and lines represent results of linear regression models with associated 95% confidence bands. Each point is colour-coded according to the volume of in-network lakes and reservoirs immediately upstream of the sampling site

TABLE 2 Statistical results of DOM composition and river site hydrology comparisons

Dependent variable	Independent variables	n	cAIC	Log likelihood	Marginal R^2	Cond. R^2	# of Sites	Overall mean R^2
FI	$\log_{10}(\tau) + \text{LV_conn} + \log_{10}(\tau)^*$ LV_conn	2213	-8195.8	3975.3	0.329	0.938	56	0.428
Freshness	$\log_{10}(\tau) + \text{LV_conn_imm} + \log_{10}(\tau)^*$ LV_conn_imm	1787	-6239.8	3053.1	0.586	0.900	41	0.781
$\log_{10}(\text{HIX})$	$\log_{10}(\tau) + \text{LV_conn} + \log_{10}(\tau)^*$ LV_conn	1888	-1711.8	803.0	0.286	0.677	45	0.438
S_R	$\log_{10}(\tau) + \text{LV_conn_imm} + \log_{10}(\tau)^*$ LV_conn_imm	2841	-8036.8	3937.0	0.605	0.857	52	0.770
SUVA_{254}	$\log_{10}(\tau) + \text{LV_conn}$	2931	5420.7	-2772.0	0.441	0.657	56	0.679

Note: Only the best-fit models, as determined by cAIC, are presented. For full statistical results, see Table S3 in Data S1. Dependent variables were spectral slope ratio (S_R), freshness index (freshness), specific ultraviolet absorbance at 254 nm (SUVA_{254}), fluorescence index (FI), and log-transformed humification index ($\log_{10}[\text{HIX}]$). Independent variables include: $\log_{10}(\tau)$ - Log-transformed FWTT of water in days; the volume of all in-network upstream lakes and reservoirs (LV_conn); the volume of in-network lakes and reservoirs immediately upstream of the sampling site (LV_conn_imm). Model conditional Aikake's Information Criterion (cAIC), log-likelihood, marginal R^2 , and conditional R^2 (Cond. R^2) are reported. We also report the R^2 for the site mean linear models (overall mean R^2) and the number of sites for which data on a given variable are available (# of sites). Not all DOM composition variables were reported at all sites. Thus, the sample size (n) reported for each variable is different.

each site, with error bars representing standard error of the mean for each site over the repeated sampling events (black circles in Figure 5). Overall, most of the model variance was captured by co-inertia dimension 1 (98.3% inertia). Consistent with the bivariate analysis, FWTT was the factor most strongly related to optical measures of DOM composition (Figure 5). FWTT was positively correlated with

Freshness Index and S_R and negatively correlated with HIX and SUVA_{254} . Lake volume and FWTT had similar model weight, but diverging influence on DOM composition. Lake area was positively correlated to Freshness Index, but more closely related to S_R (Figure 5; Table 2, Table S3 in Data S1). By contrast, FWTT was most positively correlated to Freshness Index values (Figure 5).

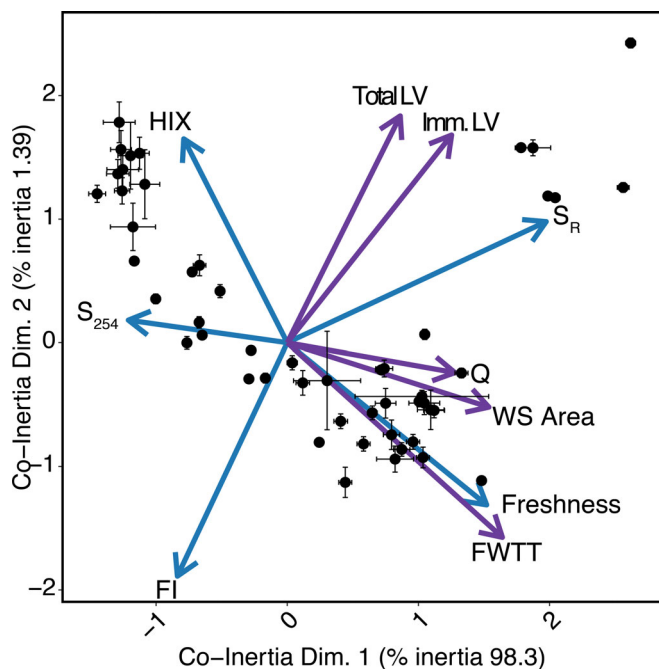


FIGURE 5 Co-inertia bi-plot comparing hydrologic and DOM composition variables. Hydrologic variables applied include: Log-transformed flow-weighted travel time in days (FWTT), log-transformed watershed area (WS area), log-transformed discharge (Q), total upstream lake and reservoir surface area (Total LV), and immediate upstream lake and reservoir surface area (Imm. LV). The DOM composition variables included specific ultraviolet absorbance at 254 nm (S_{254}), fluorescence index (FI), log-transformed HIX, freshness index (freshness), and spectral slope ratio (S_R). Co-inertia factor loadings for hydrological variables (purple arrows) and DOM composition variables (blue arrows) are presented. Mean co-inertia scores for each site are represented as black circles. Error bars represent standard error of the mean for each site across multiple samplings for dimension 1 co-inertia scores (x-axis) and dimension 2 co-inertia scores (y-axis)

4 | DISCUSSION

We found that river network FWTT is broadly correlated with DOM composition in fluvial ecosystems across the contiguous United States. We applied established relationships and concepts of river network hydrology (Leopold et al., 1995), scaling (Horton, 1945; Strahler, 1952), and flow routing (Garbrecht & Brunner, 1991) to estimate FWTT with a similar approach to a recent watershed-scale study (Peter et al., 2020). Upstream river network FWTT of water transported by a given stream or river reach can vary greatly depending on hydrologic flow status and overall stream length. Even though river network FWTT of water within a reach increased significantly with increasing upstream river length, travel time still varied substantially in a reach depending on flow status at the time of sampling (Figure S3g–i in Data S1). Variation of mean travel time within sites was sufficiently large that travel times for water under low flow (e.g., 10th percentile) at a given order typically exceed water travel times at median flow (e.g., 50th percentile) in the next higher stream order

(Figure S3j–l in Data S1). Thus, static measures of river or stream size, such as watershed area, upstream channel length, or stream order, do not capture how greatly the travel time of water through a river network changes depending on flow level.

Previous studies have demonstrated a relationship between water travel time and DOM composition at the reach or basin scale (Lynch et al., 2019; Morling et al., 2017; Peter et al., 2020; Worrall & Moody, 2014). In this study, we demonstrate that this relationship between DOM composition and FWTT is present across CONUS. Limited evidence presented here suggests that the exact slope of relationship between DOM composition and FWTT may vary between regions, but presently available data do not permit a statistically robust examination of this question. We observed a correlation between DOM composition metrics and FWTT without accounting for the variability in allochthonous DOM composition entering different river networks or differences in environmental conditions within or between river networks. In fact, we conducted an analysis on the subset of samples for which temperature was available and found no improvement in the model compared to models that incorporated only FWTT and upstream lake volume. Watershed geology (Aitkenhead & McDowell, 2000), hydrology (Jepsen et al., 2019), land use (Hosen et al., 2014; Lu et al., 2013; Wilson & Xenopoulos, 2009), and climate (de Wit et al., 2016) influence the composition of organic matter within river networks. Yet, we find that decreasing FWTT consistently leads to more aromatically dominated DOM of terrestrial origin regardless of environmental setting (Figures 3–5). In contrast to DOM composition, DOC concentrations and watershed yields were strongly correlated to discharge within individual sites, but did not demonstrate a strong correlation with FWTT across sites (Figure S6; Tables S4 and S5 in Data S1). From this analysis it seems likely that FWTT is strongly correlated to DOM composition, but that DOC concentrations and yields are driven by watershed source.

We hypothesize that river network FWTT is correlated to DOM composition in river networks because it captures the covariance of processes and gradients spanning from reaches to river basins. At a reach scale, longer travel times when discharge is lower are correlated with reduced aromatic DOM inputs due to a minimal interaction of water and organic matter-rich soil O-horizons of catchments during dry periods (Aitkenhead & McDowell, 2000; Lynch et al., 2019; Raymond & Saiers, 2010), greater light availability fueling photosynthesis and photo-oxidation (Hensley et al., 2019; Hosen et al., 2019), and more time for in-stream processing (Catalán et al., 2016; Glibert et al., 2014). By contrast, stormwater mobilizes DOM on the landscape and reduces stream travel times, pushing the transition from allochthonous to autochthonous DOM further downstream (Raymond et al., 2016; Wollheim et al., 2018). At basin scales, increased travel time is correlated with greater relative groundwater contributions from soil and bedrocks with lower permeability and greater light exposure as rivers widen downstream (Julian et al., 2008). This may explain why we found that when FWTT is short, allochthonous DOM (high HIX and S_{254}) is dominant, but as FWTT increases, the proportion of autochthonous-like DOM (with high S_R and Freshness values) increases and the proportion of allochthonous DOM decreases (Figures 3–5).

The tight link we observed between DOM metrics and FWTT suggests that downstream shifts in DOM source-composition character are driven primarily by in-channel processes, rather than allochthonous inputs. S_R increases in response to autochthonous DOM production (Y. Zhang et al., 2013) and photo-oxidation (Hansen et al., 2016; Helms et al., 2008). By contrast, Freshness Index values increase with autochthonous primary and secondary production (Hosen et al., 2021), but not photo-oxidation (Hansen et al., 2016). The observed decrease in $SUVA_{254}$ values, which are indicators of aromatic compounds in DOM (Weishaar et al., 2003), with increased FWTT provides evidence that terrestrial allochthonous DOM becomes increasingly less prevalent over time. This may indicate photo-oxidation of these compounds given that high $SUVA_{254}$ DOM is generally resistant to biodegradation, but is readily photo-oxidized by sunlight (Tranvik & Bertilsson, 2008; Ward et al., 2017). Increased contribution of groundwater in large rivers during low flows may also help make riverine allochthonous terrestrial DOM appear more autochthonous at long travel times, yet the importance of this groundwater DOM may be quite variable (Fellman et al., 2014; Hosen et al., 2021).

Increasing lake and reservoir volume had a similar impact to FWTT, increasing the dominance of autochthonous-like DOM. Lake volume explains residuals for sites with high amounts of upstream volume (Figures 3 and 4 and Figure S8 in Data S1). For Yukon and St. Lawrence sites, we found that S_R values were consistent with expectations based on the system. For example, the St. Lawrence River site had the highest S_R values of any site in this study, consistent with the expectation of long water travel time through the Great Lakes (Figure S8 in Data S1). In contrast to river network FWTT, we found that only including the volume of lakes and reservoirs immediately upstream of the study site was better at predicting DOM composition than total upstream lake and reservoir volume in some cases. Such an observation can be explained if the bioavailability of DOM produced in lakes and reservoirs is generally high, leading to short uptake lengths within river networks. High rates of autochthonous primary production and photodegradation of aromatic DOM results in delivery of autochthonous, photodegraded DOM from lakes to streams and rivers downstream (Larson et al., 2007) due to an enhanced light field (Julian et al., 2013). This lacustrine DOM is thus highly labile and can be quickly taken up by microbial communities (Chróst et al., 1989; Mostovaya et al., 2016; Yoon et al., 2021) and the influence of lakes and reservoirs on DOM composition may disappear quickly as water moves downstream. Thus, the signal of lake processes on DOM composition may be lost downstream if all the lake-associated DOM is converted to biomass, mineralized, or transformed into dissolved compounds that resemble riverine DOM.

Multivariate analysis confirmed that changes to DOM composition linked to lake and reservoirs were subtly different compared to those associated with FWTT. Both lake and reservoir volume and FWTT were related to increasing levels of autochthonous DOM, but each process impacted DOM composition in slightly different ways (Figure 5). These results are intriguing because they suggest that the three measures of autochthony reported here—Freshness Index, S_R ,

and FI—measure fractions of the overall DOM pool that are result from distinct ecosystem processes.

Estimates of FWTT correlated to DOM variability, but we recognize that our estimates likely underestimate total FWTT due to contributions from groundwater, perfluvial retention, and eddy storage (Allen, David et al., 2018), yet our findings are generally consistent with recent research indicating much of global streamflow is less than 3 months old (Jasechko et al., 2016). Further, how travel time through different parts of river corridors impacts DOM composition and fluxes remains to be seen. This model was built using the NHDPlus dataset, which is a remarkable resource, but does not capture a larger proportion of headwater stream network length (Allen & Pavelsky, 2018). Further, the complexity of river network hydrology (e.g., the influence of geomorphology on the statistical distribution of river network FWTT) cannot be fully captured by our parsimonious model. Abstraction was required to quantify the influence of lake and reservoir travel time. Despite the recognition that these water bodies are dynamic systems with preferential flowpaths and travel times that change with flow level and temperature (Gardner et al., 2019; Schmadel et al., 2018), we were unable to identify an approach to reliably estimate travel time for many lakes and reservoirs with any reliability without measuring how thermal stratification and bathymetry influence travel times in many individual systems.

The mechanism(s) and relative importance of the processes that drive the transition of DOM composition from terrestrial to autochthonous-like composition is still unclear. Recent continental-scale analysis of DOM concentrations suggests that riverine DOM concentrations are in part regulated biologically (Creed et al., 2015), indicating biological activity changes DOM composition. Yet, other analysis suggests DOM transport is conservative (Moatar et al., 2017), and groundwater inputs change composition.

Interestingly, studies of ^{14}C -DOC indicate DOM age increases with increasing autochthonous DOM character (Butman & Raymond, 2011) and watershed area (Fellman et al., 2014), but this is not necessarily an indication of age of fixation. Autochthonous production using groundwater-aged DIC will generate DOM with ^{14}C -DOC that appears aged, but is young and recently produced. Further, we note that while the present study reports a trend from allochthonous-like to autochthonous-like DOM related to FWTT, this does not necessarily indicate that bioavailability of this organic matter increases as well (Fellman et al., 2014).

We hypothesize that the freshwater DOM composition continuum (Vannote et al., 1980) is broadly linked to FWTT, particularly in temperate watersheds where temperature co-varies with discharge. While regional variables including temperature, available substrates, microbial metabolism, groundwater inputs, and a multitude of other factors control DOM uptake and production in rivers, our findings indicate that FWTT explains a large proportion of DOM composition at a national scale. By contrast, DOC concentrations and fluxes were not. We argue that our models of river network FWTT provide a useful tool to understand how riverine processes control DOM composition in drainage networks from headwaters to large rivers draining to coastal oceans.

ACKNOWLEDGEMENTS

We are grateful to the groundbreaking work of George Aiken and Kenna D. Butler, who were the architects of the of the National Water Quality Network (NWQN) that made this work possible. This work is supported by National Science Foundation Program Grants from Macrosystems (1340749, 1442140, and 1824613) and Division of Environmental Biology (1457549). We thank Matthew Miller, and two anonymous reviewers for feedback that improved the manuscript. Any use of trade, firm, or product names is for descriptive purposes only and does not imply endorsement by the U.S. Government.

DATA AVAILABILITY STATEMENT

USGS data are available at <https://doi.org/10.5066/P9PYJVHS> (Breitmeyer et al., 2019). Other data are available from sources cited in the manuscript. A compilation of data used for analysis is available as Data S2.

ORCID

Jacob D. Hosen  <https://orcid.org/0000-0003-2559-0687>

George H. Allen  <https://orcid.org/0000-0001-8301-5301>

Giuseppe Amatuli  <https://orcid.org/0000-0002-8341-2830>

Byron C. Crump  <https://orcid.org/0000-0001-7062-1273>

YueHan Lu  <https://orcid.org/0000-0002-0536-532X>

Jérôme P. Payet  <https://orcid.org/0000-0002-9862-0624>

Brett A. Poulin  <https://orcid.org/0000-0002-5555-7733>

Aron Stubbins  <https://orcid.org/0000-0002-3994-1946>

Byungman Yoon  <https://orcid.org/0000-0002-8959-3855>

Peter A. Raymond  <https://orcid.org/0000-0002-8564-7860>

REFERENCES

- Aitkenhead, J. A., & McDowell, W. H. (2000). Soil C:N ratio as a predictor of annual riverine DOC flux at local and global scales. *Global Biogeochemical Cycles*, 14(1), 127–138. <https://doi.org/10.1029/1999GB900083>
- Allen, G. H., David, C. H., Andreadis, K. M., Hossain, F., & Famiglietti, J. S. (2018). Global estimates of river flow wave travel times and implications for low-latency satellite data. *Geophysical Research Letters*, 45, 7551–7560. <https://doi.org/10.1029/2018GL077914>
- Allen, G. H., & Pavelsky, T. M. (2018). Global extent of rivers and streams. *Science*, 361(6402), 585–588. <https://doi.org/10.1126/science.aat0636>
- Allen, G. H., Pavelsky, T. M., Barefoot, E. A., Lamb, M. P., Butman, D., Tashie, A., & Gleason, C. J. (2018). Similarity of stream width distributions across headwater systems. *Nature Communications*, 9(1), 610. <https://doi.org/10.1038/s41467-018-02991-w>
- Aluwihare, L. I., & Repeta, D. J. (1999). A comparison of the chemical characteristics of oceanic DOM and extracellular DOM produced by marine algae. *Marine Ecology Progress Series*, 186, 105–117. <https://doi.org/10.3354/meps186105>
- Barber, C. A., & Gleason, C. J. (2018). Verifying the prevalence, properties, and congruent hydraulics of at-many-stations hydraulic geometry (AMHG) for rivers in the continental United States. *Journal of Hydrology*, 556, 625–633. <https://doi.org/10.1016/j.jhydrol.2017.11.038>
- Bartoń, K. (2018). *MuMIn: Multi-model inference*. Retrieved from <https://CRAN.R-project.org/package=MuMIn>
- Bates, D., Mächler, M., Bolker, B., & Walker, S. (2015). Fitting linear mixed-effects models using lme4. *Journal of Statistical Software*, 67(1), 1–48. <https://doi.org/10.18637/jss.v067.i01>
- Bernhardt, E. S., Heffernan, J. B., Grimm, N. B., Stanley, E. H., Harvey, J. W., Arroita, M., Appling, A. P., Cohen, M. J., McDowell, W. H., Hall, R. O., Read, J. S., Roberts, B. J., Stets, E. G., & Yackulic, C. B. (2018). The metabolic regimes of flowing waters: Metabolic regimes. *Limnology and Oceanography*, 63(S1), S99–S118. <https://doi.org/10.1002/lno.10726>
- Bernhardt, E. S., Likens, G. E., Buso, D. C., & Driscoll, C. T. (2003). In-stream uptake dampens effects of major forest disturbance on watershed nitrogen export. *Proceedings of the National Academy of Sciences of the United States of America*, 100(18), 10304–10308. <https://doi.org/10.1073/pnas.1233676100>
- Bertilsson, S., & Jones, J. B., Jr. (2002). Supply of dissolved organic matter to aquatic ecosystems: Autochthonous sources. In *Aquatic ecosystems: Interactivity of dissolved organic matter*. Academic Press.
- Boyer, J. N., Dailey, S. K., Gibson, P. J., Rogers, M. T., & Mir-Gonzalez, D. (2006). The role of dissolved organic matter bioavailability in promoting phytoplankton blooms in Florida Bay. *Hydrobiologia*, 569(1), 71–85. <https://doi.org/10.1007/s10750-006-0123-2>
- Boyle, E. S., Guerriero, N., Thiallet, A., Vecchio, R. D., & Blough, N. V. (2009). Optical properties of humic substances and CDOM: Relation to structure. *Environmental Science & Technology*, 43(7), 2262–2268. <https://doi.org/10.1021/es803264g>
- Breitmeyer, S. E., Aiken, G. R., & Poulin, B. A. (2019). *Dissolved organic carbon concentration and dissolved organic matter characteristics in surface water samples from the U.S. Geological Survey National Water Quality Network rivers, 2008 to 2018*. Retrieved from <https://doi.org/10.5066/P9PYJVHS>
- Bukovsky, M. S. (2011). *Masks for the Bukovsky regionalization of North America, Regional Integrated Sciences Collective, Institute for Mathematics Applied to Geosciences*. National Center for Atmospheric Research.
- Burns, M. A., Barnard, H. R., Gabor, R. S., McKnight, D. M., & Brooks, P. D. (2016). Dissolved organic matter transport reflects hillslope to stream connectivity during snowmelt in a montane catchment. *Water Resources Research*, 52(6), 4905–4923. <https://doi.org/10.1002/2015WR017878>
- Butman, D., & Raymond, P. A. (2011). Significant efflux of carbon dioxide from streams and rivers in the United States. *Nature Geoscience*, 4(12), 839–842. <https://doi.org/10.1038/ngeo1294>
- Castro, J. M., & Jackson, P. L. (2001). Bankfull discharge recurrence intervals and regional hydraulic geometry relationships: Patterns in the Pacific Northwest, USA. *JAWRA Journal of the American Water Resources Association*, 37(5), 1249–1262. <https://doi.org/10.1111/j.1752-1688.2001.tb03636.x>
- Catalán, N., Marcé, R., Kothawala, D. N., & Tranvik, L. J. (2016). Organic carbon decomposition rates controlled by water retention time across inland waters. *Nature Geoscience*, 9(7), 501–504. <https://doi.org/10.1038/ngeo2720>
- Chróst, R. J., Münster, U., Rai, H., Albrecht, D., Witzel, P. K., & Overbeck, J. (1989). Photosynthetic production and exoenzymatic degradation of organic matter in the euphotic zone of a eutrophic lake. *Journal of Plankton Research*, 11(2), 223–242. <https://doi.org/10.1093/plankt/11.2.223>
- Church, M., & Mark, D. M. (1980). On size and scale in geomorphology. *Progress in Physical Geography: Earth and Environment*, 4(3), 342–390. <https://doi.org/10.1177/030913338000400302>
- Cory, R. M., Miller, M. P., McKnight, D. M., Guerard, J. J., & Miller, P. L. (2010). Effect of instrument-specific response on the analysis of fulvic acid fluorescence spectra. *Limnology and Oceanography: Methods*, 8, 67–78.
- Creed, I. F., McKnight, D. M., Pellerin, B. A., Green, M. B., Bergamaschi, B. A., Aiken, G. R., Burns, D. A., Findlay, S. E. G., Shanley, J. B., Striegl, R. G., Aulenbach, B. T., Clow, D. W., Laudon, H., McGlynn, B. L., McGuire, K. J., Smith, R. A., & Stackpole, S. M. (2015). The river as a chemostat: Fresh perspectives on dissolved organic matter flowing down the river continuum. *Canadian Journal of Fisheries*

- and *Aquatic Sciences*, 72(8), 1272–1285. <https://doi.org/10.1139/cjfas-2014-0400>
- de Wit, H. A., Valinia, S., Weyhenmeyer, G. A., Fütter, M. N., Kortelainen, P., Austnes, K., Hessen, D. O., Råike, A., Laudon, H., & Vuorenmaa, J. (2016). Current browning of surface waters will be further promoted by wetter climate. *Environmental Science & Technology Letters*, 3(12), 430–435. <https://doi.org/10.1021/acs.estlett.6b00396>
- Dittmar, T., & Stubbins, A. (2014). Dissolved organic matter in aquatic systems. In *Treatise on geochemistry* (pp. 125–156). Elsevier. Retrieved from <https://doi.org/10.1016/B978-0-08-095975-7.01010-X>
- Doledec, S., & Chessel, D. (1994). Co-inertia analysis: An alternative method for studying species-environment relationships. *Freshwater Biology*, 31(3), 277–294. <https://doi.org/10.1111/j.1365-2427.1994.tb01741.x>
- Dray, S., Chessel, D., & Thioulouse, J. (2003). Co-Inertia analysis and the linking of ecological data tables. *Ecology*, 84(11), 3078–3089. <https://doi.org/10.1890/03-0178>
- Dray, S., & Dufour, A.-B. (2007). The ade4 package: Implementing the duality diagram for ecologists. *Journal of Statistical Software*, 22(4), 1–20. <https://doi.org/10.18637/jss.v022.i04>
- Dunne, T., & Leopold, L. B. (1978). *Water in environmental planning*. Retrieved from https://books-google-com.proxy-um.researchport.umd.edu/books/about/Water_in_Environmental_Planning.html?id=d7WEkcTNk6EC
- Febria, C. M., Hosen, J. D., Crump, B. C., Palmer, M. A., & Williams, D. D. (2015). Microbial responses to changes in flow status in temporary headwater streams: a cross-system comparison. *Aquatic Microbiology*, 6, 522. <https://doi.org/10.3389/fmicb.2015.00522>
- Fellman, J. B., Hood, E., Edwards, R. T., & D'Amore, D. V. (2009). Changes in the concentration, biodegradability, and fluorescent properties of dissolved organic matter during stormflows in coastal temperate watersheds. *Journal of Geophysical Research*, 114(G1), G01021. <https://doi.org/10.1029/2008JG000790>
- Fellman, J. B., Spencer, R. G. M., Raymond, P. A., Pettit, N. E., Skrzypek, G., Hernes, P. J., & Grierson, P. F. (2014). Dissolved organic carbon biolability decreases along with its modernization in fluvial networks in an ancient landscape. *Ecology*, 95(9), 2622–2632. <https://doi.org/10.1890/13-1360.1>
- Garbrecht, J., & Brunner, G. W. (1991). *A Muskingum-Cunge channel flow routing method for drainage networks*. Hydrologic Engineering Center.
- Gardner, J. R., Pavelsky, T. M., & Doyle, M. W. (2019). The abundance, size, and spacing of lakes and reservoirs connected to river networks. *Geophysical Research Letters*, 46(5), 2592–2601. <https://doi.org/10.1029/2018GL080841>
- Gleason, C. J., & Smith, L. C. (2014). Toward global mapping of river discharge using satellite images and at-many-stations hydraulic geometry. *Proceedings of the National Academy of Sciences of the United States of America*, 111(13), 4788–4791. <https://doi.org/10.1073/pnas.1317606111>
- Gleason, C. J., Smith, L. C., & Lee, J. (2014). Retrieval of river discharge solely from satellite imagery and at-many-stations hydraulic geometry: Sensitivity to river form and optimization parameters. *Water Resources Research*, 50(12), 9604–9619. <https://doi.org/10.1002/2014WR016109>
- Glibert, P. M., Dugdale, R. C., Wilkerson, F., Parker, A. E., Alexander, J., Antell, E., Blaser, S., Johnson, A., Lee, J., Lee, T., Murasko, S., & Strong, S. (2014). Major – but rare – spring blooms in 2014 in San Francisco Bay Delta, California, a result of the long-term drought, increased residence time, and altered nutrient loads and forms. *Journal of Experimental Marine Biology and Ecology*, 460, 8–18. <https://doi.org/10.1016/j.jembe.2014.06.001>
- GRASS Development Team. (2018). Geographic Resources Analysis Support System (GRASS GIS) Software. Open Source Geospatial Foundation: USA. Available at: <https://grass.osgeo.org>
- Greven, S., & Kneib, T. (2010). On the behaviour of marginal and conditional AIC in linear mixed models. *Biometrika*, 97(4), 773–789. <https://doi.org/10.1093/biomet/asq042>
- Hall, R. O., & Meyer, J. L. (1998). The trophic significance of bacteria in a detritus-based stream food web. *Ecology*, 79(6), 1995–2012.
- Hall, R. O., Yackulic, C. B., Kennedy, T. A., Yard, M. D., Rosi-Marshall, E. J., Voichick, N., & Behn, K. E. (2015). Turbidity, light, temperature, and hydropeaking control primary productivity in the Colorado River, Grand Canyon. *Limnology and Oceanography*, 60(2), 512–526. <https://doi.org/10.1002/lno.10031>
- Hansen, A. M., Kraus, T. E. C., Pellerin, B. A., Fleck, J. A., Downing, B. D., & Bergamaschi, B. A. (2016). Optical properties of dissolved organic matter (DOM): Effects of biological and photolytic degradation. *Limnology and Oceanography*, 61(3), 1015–1032. <https://doi.org/10.1002/lno.10270>
- Hay, L. E. (2019). *Application of the national hydrologic model infrastructure with the precipitation-runoff modeling system (NHM-PRMS), by HRU calibrated version*. Retrieved from <https://doi.org/10.5066/p9nm8k8w>
- Helms, J. R., Mao, J., Stubbins, A., Schmidt-Rohr, K., Spencer, R. G. M., Hernes, P. J., & Mopper, K. (2014). Loss of optical and molecular indicators of terrigenous dissolved organic matter during long-term photobleaching. *Aquatic Sciences*, 76(3), 353–373. <https://doi.org/10.1007/s00027-014-0340-0>
- Helms, J. R., Stubbins, A., Ritchie, J. D., Minor, E. C., Kieber, D. J., & Mopper, K. (2008). Absorption spectral slopes and slope ratios as indicators of molecular weight, source, and photobleaching of chromophoric dissolved organic matter. *Limnology and Oceanography*, 53(3), 955–969.
- Hensley, R. T., Kirk, L., Spangler, M., Gooseff, M. N., & Cohen, M. J. (2019). Flow extremes as spatiotemporal control points on river solute fluxes and metabolism. *Journal of Geophysical Research: Biogeosciences*, 124, 537–555. <https://doi.org/10.1029/2018JG004738>
- Hornberger, G. M., Bencala, K. E., & McKnight, D. M. (1994). Hydrological controls on dissolved organic carbon during snowmelt in the Snake River near Montezuma, Colorado. *Biogeochemistry*, 25(3), 147–165. <https://doi.org/10.1007/BF00024390>
- Horton, R. E. (1945). Erosional development of streams and their drainage basins; hydrological approach to quantitative morphology. *Geological Society of America Bulletin*, 56(3), 275. [https://doi.org/10.1130/0016-7606\(1945\)56\[275:EDOSAT\]2.0.CO;2](https://doi.org/10.1130/0016-7606(1945)56[275:EDOSAT]2.0.CO;2)
- Hosen, J. D., Aho, K. S., Appling, A. P., Creech, E. C., Fair, J. H., Hall, R. O., Kyzivat, E. D., Lowenthal, R. S., Matt, S., Morrison, J., Saiers, J. E., Shanley, J. B., Weber, L. C., Yoon, B., & Raymond, P. A. (2019). Enhancement of primary production during drought in a temperate watershed is greater in larger rivers than headwater streams. *Limnology and Oceanography*, 64, 1458–1472. <https://doi.org/10.1002/lno.11127>
- Hosen, J. D., Aho, K. S., Fair, J. H., Kyzivat, E. D., Matt, S., Morrison, J., Stubbins, A., Weber, L. C., Yoon, B., & Raymond, P. A. (2021). Source switching maintains dissolved organic matter chemostasis across discharge levels in a large temperate river network. *Ecosystems*, 24, 227–247. <https://doi.org/10.1007/s10021-020-00514-7>
- Hosen, J. D., Armstrong, A. W., & Palmer, M. A. (2018). Dissolved organic matter variations in coastal plain wetland watersheds: The integrated role of hydrological connectivity, land use, and seasonality. *Hydrological Processes*, 32, 1664–1681. <https://doi.org/10.1002/hyp.11519>
- Hosen, J. D., Febria, C. M., Crump, B. C., & Palmer, M. A. (2017). Watershed urbanization linked to differences in stream bacterial community composition. *Frontiers in Microbiology*, 8, 1452. <https://doi.org/10.3389/fmicb.2017.01452>
- Hosen, J. D., McDonough, O. T., Febria, C. M., & Palmer, M. A. (2014). Dissolved organic matter quality and bioavailability changes across an urbanization gradient in headwater streams. *Environmental Science & Technology*, 48(14), 7817–7824. <https://doi.org/10.1021/es501422z>
- Inamdar, S., Dhillon, G., Singh, S., Dutta, S., Levia, D., Scott, D., Mitchell, M., Van Stan, J., & McHale, P. (2013). Temporal variation in end-member chemistry and its influence on runoff mixing patterns in a forested, Piedmont catchment. *Water Resources Research*, 49(4), 1828–1844. <https://doi.org/10.1002/wrcr.20158>

- Inamdar, S., Singh, S., Dutta, S., Levia, D., Mitchell, M., Scott, D., Bais, H., & McHale, P. (2011). Fluorescence characteristics and sources of dissolved organic matter for stream water during storm events in a forested mid-Atlantic watershed. *Journal of Geophysical Research*, 116 (G3), G03043. <https://doi.org/10.1029/2011JG001735>
- Jasechko, S., Kirchner, J. W., Welker, J. M., & McDonnell, J. J. (2016). Substantial proportion of global streamflow less than three months old. *Nature Geoscience*, 9(2), 126–129. <https://doi.org/10.1038/ngeo2636>
- Jepsen, S. M., Harmon, T. C., Sadro, S., Reid, B., & Chandra, S. (2019). Water residence time (age) and flow path exert synchronous effects on annual characteristics of dissolved organic carbon in terrestrial runoff. *Science of the Total Environment*, 656, 1223–1237. <https://doi.org/10.1016/j.scitotenv.2018.11.392>
- Julian, J. P., Davies-Colley, R. J., Gallegos, C. L., & Tran, T. V. (2013). Optical water quality of inland waters: A landscape perspective. *Annals of the Association of American Geographers*, 103(2), 309–318. <https://doi.org/10.1080/00045608.2013.754658>
- Julian, J. P., Doyle, M. W., & Stanley, E. H. (2008). Empirical modeling of light availability in rivers. *Journal of Geophysical Research*, 113, G03022. <https://doi.org/10.1029/2007JG000601>
- Kamjunke, N., Lechtenfeld, O. J., & Herzsprung, P. (2020). Quality of dissolved organic matter driven by autotrophic and heterotrophic microbial processes in a large river. *Water*, 12(6), 1577. <https://doi.org/10.3390/w12061577>
- Kaplan, L. A., & Cory, R. M. (2016). Dissolved organic matter in stream ecosystems: Forms, functions, and fluxes of watershed tea. In J. B. Jones & E. H. Stanley (Eds.), *Stream ecosystems in a changing environment* (pp. 241–320). Academic Press. chap. 6. Retrieved from <https://doi.org/10.1016/B978-0-12-405890-3.00006-3>
- Kellerman, A. M., Kothawala, D. N., Dittmar, T., & Tranvik, L. J. (2015). Persistence of dissolved organic matter in lakes related to its molecular characteristics. *Nature Geoscience*, 8(6), 454–457. <https://doi.org/10.1038/ngeo2440>
- King, K., Cheruvilil, K. S., & Pollard, A. (2019). Drivers and spatial structure of abiotic and biotic properties of lakes, wetlands, and streams at the national scale. *Ecological Applications*, 29, e01957. <https://doi.org/10.1002/eap.1957>
- Kirchner, J. W. (2019). Quantifying new water fractions and transit time distributions using ensemble hydrograph separation: Theory and benchmark tests. *Hydrology and Earth System Sciences*, 23(1), 303–349. <https://doi.org/10.5194/hess-23-303-2019>
- Koenig, L. E., Helton, A. M., Savoy, P., Bertuzzo, E., Heffernan, J. B., Hall, R. O., & Bernhardt, E. S. (2019). Emergent productivity regimes of river networks. *Limnology and Oceanography Letters*, 4, 173–181. <https://doi.org/10.1002/lol2.10115>
- Kothawala, D. N., Kellerman, A. M., Catalán, N., & Tranvik, L. J. (2020). Organic matter degradation across ecosystem boundaries: The need for a unified conceptualization. *Trends in Ecology & Evolution*, 36, 113–122. <https://doi.org/10.1016/j.tree.2020.10.006>
- Kulkarni, H. V., Mladenov, N., Johannesson, K. H., & Datta, S. (2017). Contrasting dissolved organic matter quality in groundwater in Holocene and Pleistocene aquifers and implications for influencing arsenic mobility. *Applied Geochemistry*, 77, 194–205. <https://doi.org/10.1016/j.apgeochem.2016.06.002>
- Kuznetsova, A., Brockhoff, P. B., & Christensen, R. H. B. (2017). lmerTest package: Tests in linear mixed effects models. *Journal of Statistical Software*, 82(13), 1–26. <https://doi.org/10.18637/jss.v082.i13>
- Larson, J. H., Frost, P. C., Zheng, Z., Johnston, C. A., Bridgman, S. D., Lodge, D. M., & Lamberti, G. A. (2007). Effects of upstream lakes on dissolved organic matter in streams. *Limnology and Oceanography*, 52 (1), 60–69. <https://doi.org/10.4319/lo.2007.52.1.0060>
- Lefcheck, J. S. (2016). piecewiseSEM: Piecewise structural equation modeling in R for ecology, evolution, and systematics. *Methods in Ecology and Evolution*, 7(5), 573–579. <https://doi.org/10.1111/2041-210X.12512>
- Leopold, L. B., & Maddock, T. (1953). The hydraulic geometry of stream channels and some physiographic implications. US Government Printing Office.
- Leopold, L. B., Wolman, M. G., & Miller, J. P. (1995). *Fluvial processes in geomorphology*. Dover Publications.
- Li, M., Peng, C., Wang, M., Xue, W., Zhang, K., Wang, K., Shi, G., & Zhu, Q. (2017). The carbon flux of global rivers: A re-evaluation of amount and spatial patterns. *Ecological Indicators*, 80, 40–51. <https://doi.org/10.1016/j.ecolind.2017.04.049>
- Lu, Y., Bauer, J. E., Canuel, E. A., Yamashita, Y., Chambers, R. M., & Jaffé, R. (2013). Photochemical and microbial alteration of dissolved organic matter in temperate headwater streams associated with different land use. *Journal of Geophysical Research: Biogeosciences*, 118(2), 566–580.
- Lynch, L. M., Sutfin, N. A., Fegal, T. S., Boot, C. M., Covino, T. P., & Wallenstein, M. D. (2019). River channel connectivity shifts metabolite composition and dissolved organic matter chemistry. *Nature Communications*, 10(1), 1–11. <https://doi.org/10.1038/s41467-019-08406-8>
- Maranger, R., Jones, S. E., & Cotner, J. B. (2018). Stoichiometry of carbon, nitrogen, and phosphorus through the freshwater pipe. *Limnology and Oceanography Letters*, 3(3), 89–101. <https://doi.org/10.1002/lol2.10080>
- Massicotte, P., Asmala, E., Stedmon, C., & Markager, S. (2017). Global distribution of dissolved organic matter along the aquatic continuum: Across rivers, lakes and oceans. *Science of the Total Environment*, 609, 180–191. <https://doi.org/10.1016/j.scitotenv.2017.07.076>
- Mauricio Zambrano-Bigiarini. (2017). hydroTSM: Time Series Management, Analysis and Interpolation for Hydrological Modelling. <https://github.com/hzamban/hydroTSM>
- McKay, L., Bondelid, T., Dewald, T., Johnston, J., Moore, R., & Rea, A. (2012). *NHD Plus Version 2: User guide*. United States Environmental Protection Agency and United States Geological Survey
- McKnight, D. M., Boyer, E. W., Westerhoff, P. K., Doran, P. T., Kulbe, T., & Andersen, D. T. (2001). Spectrofluorometric characterization of dissolved organic matter for indication of precursor organic material and aromaticity. *Limnology and Oceanography*, 46(1), 38–48.
- Miller, M. P., Boyer, E. W., McKnight, D. M., Brown, M. G., Gabor, R. S., Hunsaker, C. T., Iavorivska, L., Inamdar, S., Johnson, D. W., Kaplan, L. A., Lin, H., McDowell, W. H., & Perdrial, J. N. (2016). Variation of organic matter quantity and quality in streams at Critical Zone Observatory watersheds. *Water Resources Research*, 52(10), 8202–8216. <https://doi.org/10.1002/2016WR018970>
- Moatar, F., Abbott, B. W., Minaudo, C., Curie, F., & Pinay, G. (2017). Elemental properties, hydrology, and biology interact to shape concentration-discharge curves for carbon, nutrients, sediment, and major ions. *Water Resources Research*, 53(2), 1270–1287. <https://doi.org/10.1002/2016WR019635>
- Moran, M. A., & Zepp, R. G. (1997). Role of photoreactions in the formation of biologically labile compounds from dissolved organic matter. *Limnology and Oceanography*, 42(6), 1307–1316. <https://doi.org/10.4319/lo.1997.42.6.1307>
- Morling, K., Herzsprung, P., & Kamjunke, N. (2017). Discharge determines production of, decomposition of and quality changes in dissolved organic carbon in pre-dams of drinking water reservoirs. *Science of the Total Environment*, 577, 329–339. <https://doi.org/10.1016/j.scitotenv.2016.10.192>
- Mosher, J. J., Kaplan, L. A., Podgorski, D. C., McKenna, A. M., & Marshall, A. G. (2015). Longitudinal shifts in dissolved organic matter chemogeography and chemodiversity within headwater streams: A river continuum reprise. *Biogeochemistry*, 124(1), 371–385. <https://doi.org/10.1007/s10533-015-0103-6>
- Mostovaya, A., Koehler, B., Guillemette, F., Brunberg, A.-K., & Tranvik, L. J. (2016). Effects of compositional changes on reactivity continuum and decomposition kinetics of lake dissolved organic matter. *Journal of Geophysical Research: Biogeosciences*, 121, 1733–1746. <https://doi.org/10.1002/2016JG003359>

- Nakagawa, S., Johnson, P. C. D., & Schielzeth, H. (2017). The coefficient of determination R^2 and intra-class correlation coefficient from generalized linear mixed-effects models revisited and expanded. *Journal of the Royal Society Interface*, 14(134), 20170213. <https://doi.org/10.1098/rsif.2017.0213>
- Nakagawa, S., & Schielzeth, H. (2013). A general and simple method for obtaining R^2 from generalized linear mixed-effects models. *Methods in Ecology and Evolution*, 4(2), 133–142. <https://doi.org/10.1111/j.2041-210x.2012.00261.x>
- O'Donnell, J. A., Aiken, G. R., Walvoord, M. A., & Butler, K. D. (2012). Dissolved organic matter composition of winter flow in the Yukon River basin: Implications of permafrost thaw and increased groundwater discharge. *Global Biogeochemical Cycles*, 26(4), 2012GB0E06. <https://doi.org/10.1029/2012GB004341>
- Ohno, T. (2002). Fluorescence inner-filtering correction for determining the humification index of dissolved organic matter. *Environmental Science & Technology*, 36(4), 742–746. <https://doi.org/10.1021/es0155276>
- Paerl, H. W., Pinckney, J. L., Fear, J. M., & Peierls, B. L. (1998). Ecosystem responses to internal and watershed organic matter loading: Consequences for hypoxia in the eutrophying Neuse River Estuary, North Carolina, USA. *Marine Ecology Progress Series*, 166, 17–25.
- Palmer, M., & Ruhí, A. (2019). Linkages between flow regime, biota, and ecosystem processes: Implications for river restoration. *Science*, 365(6459), eaaw2087. <https://doi.org/10.1126/science.aaw2087>
- Parlanti, E., Wörz, K., Geoffroy, L., & Lamotte, M. (2000). Dissolved organic matter fluorescence spectroscopy as a tool to estimate biological activity in a coastal zone submitted to anthropogenic inputs. *Organic Geochemistry*, 31(12), 1765–1781. [https://doi.org/10.1016/S0146-6380\(00\)00124-8](https://doi.org/10.1016/S0146-6380(00)00124-8)
- Peter, H., Singer, G., Ulseth, A. J., Dittmar, T., Prairie, Y. T., & Battin, T. J. (2020). Travel time and source variation explain the molecular transformation of dissolved organic matter in an alpine stream network. *Journal of Geophysical Research: Biogeosciences*, 125(8). <http://doi.org/10.1029/2019jg005616>
- Poulsen, J. R., Sebok, E., Duque, C., Tetzlaff, D., & Engesgaard, P. K. (2015). Detecting groundwater discharge dynamics from point-to-catchment scale in a lowland stream: Combining hydraulic and tracer methods. *Hydrology and Earth System Sciences*, 19(4), 1871–1886. <https://doi.org/10.5194/hess-19-1871-2015>
- Prein, A. F., Holland, G. J., Rasmussen, R. M., Clark, M. P., & Tye, M. R. (2016). Running dry: The U.S. Southwest's drift into a drier climate state. *Geophysical Research Letters*, 43(3), 1272–1279. <https://doi.org/10.1002/2015GL066727>
- Raymond, P. A., & Saiers, J. E. (2010). Event controlled DOC export from forested watersheds. *Biogeochemistry*, 100(1–3), 197–209. <https://doi.org/10.1007/s10533-010-9416-7>
- Raymond, P. A., Saiers, J. E., & Sobczak, W. V. (2016). Hydrological and biogeochemical controls on watershed dissolved organic matter transport: Pulse-shunt concept. *Ecology*, 97(1), 5–16. <https://doi.org/10.1890/14-1684.1>
- R Core Team. (2018). R: A Language and Environment for Statistical Computing. R Foundation for Statistical Computing: Vienna, Austria. Available at: <https://www.R-project.org/>
- Repeta, D. J. (2015). Chemical characterization and cycling of dissolved organic matter. In *Biogeochemistry of marine dissolved organic matter* (pp. 21–63). Elsevier. Retrieved from <https://doi.org/10.1016/B978-0-12-405940-5.00002-9>
- Saefken, B., Kneib, T., van Waveren, C.-S., & Greven, S. (2014). A unifying approach to the estimation of the conditional Akaike information in generalized linear mixed models. *Electronic Journal of Statistics*, 8(1), 201–225. <https://doi.org/10.1214/14-EJS881>
- Säfken, B., Rügamer, D., Kneib, T., & Greven, S. (2018). Conditional model selection in mixed-effects models with cAIC4. *arXiv:1803.05664 [stat]*. Retrieved from <http://arxiv.org/abs/1803.05664>
- Schmadel, N. M., Harvey, J. W., Alexander, R. B., Schwarz, G. E., Moore, R. B., Eng, K., Gomez-Velez, J. D., Boyer, E. W., & Scott, D. (2018). Thresholds of lake and reservoir connectivity in river networks control nitrogen removal. *Nature Communications*, 9(1), 2779. <https://doi.org/10.1038/s41467-018-05156-x>
- Shang, P. (2019). *Anthropogenic and environmental drivers of the input and uptake of dissolved organic matter in temperate streams* (Ph.D. Dissertation). University of Alabama.
- Shang, P., Lu, Y., Du, Y., Jaffé, R., Findlay, R. H., & Wynn, A. (2018). Climatic and watershed controls of dissolved organic matter variation in streams across a gradient of agricultural land use. *Science of the Total Environment*, 612, 1442–1453. <https://doi.org/10.1016/j.scitotenv.2017.08.322>
- Shultz, M., Pellerin, B., Aiken, G., Martin, J., & Raymond, P. (2018). High frequency data exposes nonlinear seasonal controls on dissolved organic matter in a large watershed. *Environmental Science & Technology*, 52(10), 5644–5652. <https://doi.org/10.1021/acs.est.7b04579>
- Simon, A., Dickerson, W., & Heins, A. (2004). Suspended-sediment transport rates at the 1.5-year recurrence interval for ecoregions of the United States: Transport conditions at the bankfull and effective discharge? *Geomorphology*, 58(1), 243–262. <https://doi.org/10.1016/j.geomorph.2003.07.003>
- Stedmon, C. A., Markager, S., & Bro, R. (2003). Tracing dissolved organic matter in aquatic environments using a new approach to fluorescence spectroscopy. *Marine Chemistry*, 82(3–4), 239–254. [https://doi.org/10.1016/S0304-4203\(03\)00072-0](https://doi.org/10.1016/S0304-4203(03)00072-0)
- Strahler, A. N. (1952). Hypsometric (Area-Altitude) analysis of erosional topography. *Geological Society of America Bulletin*, 63(11), 1117. [https://doi.org/10.1130/0016-7606\(1952\)63\[1117:HAAOET\]2.0.CO;2](https://doi.org/10.1130/0016-7606(1952)63[1117:HAAOET]2.0.CO;2)
- Tranvik, L. J., & Bertilsson, S. (2008). Contrasting effects of solar UV radiation on dissolved organic sources for bacterial growth. *Ecology Letters*, 4(5), 458–463. <https://doi.org/10.1046/j.1461-0248.2001.00245.x>
- United States Geological Survey. (2016). *USGS water data for the Nation*. U.S. Geological Survey National Water Information System Database. Retrieved from <https://doi.org/10.5066/F7P55KJN>
- U.S. Geological Survey. (2019). National Hydrography Dataset. 2019. <https://www.usgs.gov/core-science-systems/ngp/national-hydrography/access-national-hydrography-products>
- Vannote, R. L., Minshall, G. W., Cummins, K. W., Sedell, J. R., & Cushing, C. E. (1980). The river continuum concept. *Canadian Journal of Fisheries and Aquatic Sciences*, 37(1), 130–137. <https://doi.org/10.1139/f80-017>
- Wagner, S., Fair, J. H., Matt, S., Hosen, J. D., Raymond, P., Saiers, J., Shanley, J. B., Dittmar, T., & Stubbins, A. (2019). Molecular hysteresis: Hydrologically driven changes in riverine dissolved organic matter chemistry during a storm event. *Journal of Geophysical Research: Biogeosciences*, 124(4), 759–774. <https://doi.org/10.1029/2018JG004817>
- Ward, N. D., Bianchi, T. S., Medeiros, P. M., Seidel, M., Richey, J. E., Keil, R. G., & Sawakuchi, H. O. (2017). Where carbon goes when water flows: Carbon cycling across the aquatic continuum. *Frontiers in Marine Science*, 4, 7. <https://doi.org/10.3389/fmars.2017.00007>
- Weishaar, J. L., Aiken, G. R., Bergamaschi, B. A., Fram, M. S., Fujii, R., & Mopper, K. (2003). Evaluation of specific ultraviolet absorbance as an indicator of the chemical composition and reactivity of dissolved organic carbon. *Environmental Science & Technology*, 37(20), 4702–4708. <https://doi.org/10.1021/es030360x>
- Wilson, H. F., & Xenopoulos, M. A. (2009). Effects of agricultural land use on the composition of fluvial dissolved organic matter. *Nature Geoscience*, 2(1), 37–41. <https://doi.org/10.1038/ngeo391>
- Wollheim, W. M., Bernal, S., Burns, D. A., Czuba, J. A., Driscoll, C. T., Hansen, A. T., Hensley, R. T., Hosen, J. D., Inamdar, S., Kaushal, S. S., Koening, L. E., Lu, Y. H., Marzadri, A., Raymond, P. A., Scott, D., Stewart, R. J., Vidon, P. G., & Wohl, E. (2018). River network saturation concept: Factors influencing the balance of biogeochemical supply and demand of river networks. *Biogeochemistry*, 141(3), 503–521. <https://doi.org/10.1007/s10533-018-0488-0>

- Worrall, F., Howden, N. J. K., & Burt, T. P. (2014). A method of estimating in-stream residence time of water in rivers. *Journal of Hydrology*, 512, 274–284. <https://doi.org/10.1016/j.jhydrol.2014.02.050>
- Worrall, F., & Moody, C. S. (2014). Modeling the rate of turnover of DOC and particulate organic carbon in a UK, peat-hosted stream: Including diurnal cycling in short-residence time systems. *Journal of Geophysical Research: Biogeosciences*, 119(10), 1934–1946. <https://doi.org/10.1002/2014JG002671>
- Wünsch, U. J., Stedmon, C. A., Tranvik, L. J., & Guillemette, F. (2018). Unraveling the size-dependent optical properties of dissolved organic matter: Size-dependent optical properties of DOM. *Limnology and Oceanography*, 63(2), 588–601. <https://doi.org/10.1002/lno.10651>
- Yoon, B., Hosen, J. D., Kyzivat, E. D., Fair, J. H., Weber, L. C., Aho, K. S., Lowenthal, R., Matt, S., Sobczak, W. V., Shanley, J. B., Morrison, J., Saiers, J. E., Stubbins, A., & Raymond, P. A. (2021). Export of photolabile and photoprivable dissolved organic carbon from the Connecticut River. *Aquatic Sciences*, 83(2), 23. <https://doi.org/10.1007/s00027-021-00778-8>
- Zarnetske, J. P., Bouda, M., Abbott, B. W., Saiers, J., & Raymond, P. A. (2018). Generality of hydrologic transport limitation of watershed organic carbon flux across ecoregions of the United States. *Geophysical Research Letters*, 45(21), 11,702–11,711. <https://doi.org/10.1029/2018GL080005>
- Zhang, T., & Wang, X. (2017). Release and microbial degradation of dissolved organic matter (DOM) from the macroalgae *Ulva prolifera*. *Marine Pollution Bulletin*, 125(1–2), 192–198. <https://doi.org/10.1016/j.marpolbul.2017.08.029>
- Zhang, Y., Liu, X., Wang, M., & Qin, B. (2013). Compositional differences of chromophoric dissolved organic matter derived from phytoplankton and macrophytes. *Organic Geochemistry*, 55, 26–37. <https://doi.org/10.1016/j.orggeochem.2012.11.007>

SUPPORTING INFORMATION

Additional supporting information may be found online in the Supporting Information section at the end of this article.

How to cite this article: Hosen JD, Allen GH, Amatuli G, et al. River network travel time is correlated with dissolved organic matter composition in rivers of the contiguous United States. *Hydrological Processes*. 2021;35:e14124. <https://doi.org/10.1002/hyp.14124>